TAMPEREEN TEKNILLINEN YLIOPISTO
TAMPERE UNIVERSITY OF TECHNOLOGY

Matti Harkoma

Confinement in the Diode Laser Ignition of Energetic Materials

Julkaisu 883 • Publication 883

Tampere 2010

Tampereen teknillinen yliopisto. Julkaisu 883
Tampere University of Technology. Publication 883

Matti Harkoma

Confinement in the Diode Laser Ignition of Energetic Materials

Thesis for the degree of Doctor of Technology to be presented with due permission for public examination and criticism in Sähkötalo Building, Auditorium S1, at Tampere University of Technology, on the 10th of June 2010, at 12 noon.

Tampereen teknillinen yliopisto - Tampere University of Technology
Tampere 2010

ISBN 978-952-15-2354-0 (printed)
ISBN 978-952-15-2405-9 (PDF)
ISSN 1459-2045

Abstract

The diode laser is increasingly used as an ignition device for pyrotechnic mixtures or propellants and for explosives. The ignition properties of different energetic materials are important for understanding the ignition mechanism or choosing the best or suitable material for the current laser ignition application. One of the most important variables is the ignition energy. Thus it is reasonable to study the minimum ignition energy of many energetic materials and choose the best material among them. Other criteria may be, for example, the detonation properties of the current material as a booster or an igniter and the ageing properties of the current material.

A strong dependence between the ignition energy and the ambient pressure was observed in the results. For example, in the case of RDX98/1/1+1% carbon black the measured energy in an ambient pressure of 10 bar was 180 mJ and in an ambient pressure of 50 bar it was 32.6 mJ. Mean ignition energy densities were 29,9 J/cm^2 and 5,4 J/cm^2, respectively. The carbon black content's effect on the ignition energy is clear between 1% and 3%, the ignition energy at 2% carbon black content being 27% lower than at 1% carbon black content, and 31% lower than at 3% carbon black content. According to the experiments, the mechanical properties of the RDX pellet are fragile at 3% or higher carbon black content. Thus the optimum carbon black content may be 1,5 to 2,5%.

According to the diode laser ignition experiments with synthetic air and argon the ignition energies are essentially the same in the same confinement. These results suggest that oxygen (in synthetic air) has no remarkable reactions in the laser illuminated point of the RDX pellet or more generally in the laser illuminated point of the explosive.

For nitrogen the ignition energies are slightly higher compared with air (and also with argon) in the same pressure. This is analogous compared with the CO_2 laser ignition results at lower pressures by other authors, but at higher pressures of air

and nitrogen the experimental results of this work and of the reference are in reverse order.

Evaporated RDX and gaseous decomposition products expand and will displace synthetic air, nitrogen or argon. Initial decomposition takes place in the vapour phase of RDX and on the surface of melted RDX. Highly exothermic reactions begin in the vapour phase and are followed by more rapid decomposition in the vapour phase and in the liquid phase and ignition of RDX. The rate of the reactions is deflagration, but it accelerates to the steady state detonation in the environment of high confinement. The conclusion that can be drawn is that the ignition process is not only a solid phase reaction but a complex process where gas, liquid, and/or solid phase reactions are involved.

According to this work, the degree of confinement has a strong role in the deflagration to detonation transition ignition mechanism. Using a degree of confinement that is heavy enough, a closed and tight mechanical structure, a high enough pressure inside the device, and good absorbance, for example using carbon black in the energetic material, the ignition energy would be low enough for economically viable applications of compact diode laser igniters.

Preface

The present work was carried out in the Explosive Technology Laboratory of the Finnish Defence Forces Technical Research Centre (PVTT) and in the Department of Electronics at the Tampere University of Technology. I am very grateful to my supervisor Prof. Karri Palovuori for his support and valuable advice during this work. I would specially like to thank my colleagues M.Sc. Maija Hihkiö and M.Sc. Mari-Ella Sairiala, M.Sc. Tapio Heininen, and Lic.Phil. Timo-Jaakko Toivanen. Special thanks are due to Techn. Tellervo Vormisto and Bachelor of Laboratory Services Tiina Runsas for support and for very good teamwork as well as Techn. Petri Wallgrén for the many quality pictures in this thesis.

In the course of laser ignition research at PVTT, the author spent two months in 1997 at the Energetic Material Laboratory of FOI, in Grindsjön Tumba, Sweden, the staff of which I would like to thank, and specially Ph.D. Henric Östmark, M.Sc. Anna Pettersson, M.Sc. Nils Roman, and M.Sc. Janne Pettersson.

All the staff at the Finnish Defence Forces Research Institute of Technology receive my thanks, in particular Colonel Mika Hyytiäinen, M.Sc. Alpo Kariniemi as well as the workshop staff and my colleagues. I would like to thank Colonel Ilkka Jäppinen and Colonel Esa Lappalainen.

I would also like to thank at the Finnish Navy Ing. Commodore Arto Hakala, Ing. Commander Pekka Loivaranta and Commander Ari Kallio for the financial resources for laser ignition research at PVTT.

I would also like to thank Prof. Timo Jääskeläinen and Ph.D. Henric Östmark for their comments and remarks on this thesis.

Finally, I would like to express my deepest gratitude to my wife Sisko and my son Olli for their best possible support during this work.

Ylöjärvi, December 2009

Matti Harkoma

Contents

List of Abbreviations and Symbols

AD	Ammonium Perchlorate
BKW	Becker-Kistiakowsky-Wilson
CJ	Chapman-Jouguet
C-J State	Chapman-Jouguet State
DATB	Diaminotrinitrobenzene
DDT	Deflagration to Detonation Transition
DSC	Differential Scanning Calorimeter
FPX	Forcit Plastic-Bonded Explosive
HMX	Octogen
HNS	Hexanitrostilbene
IR	Infra Red
JWL	Jones-Wilkins-Lee
LI/MS	Laser Ignition with Mass Spectroscopy
LIF	Laser Induced Fluorescence
NIR	Near Infra Red
NM	Nitromethane
NTO	Nitrotriazolone
NQ	Nitroguanidine
P1	Pentolite One
PBX	Plastic-Bonded Explosive
PETN	Pentolite
PVTT	Puolustusvoimien Teknillinen Tutkimuslaitos
RDX	Royal Demolition Explosive, Hexogen
STD	Shock to Detonation Transition
TG	Thermo Gravimetric
TNT	Trinitrotoluene
TATB	Triaminotrinitrobentzene
UV	Ultra Violet
VIS	Visible
YAG	Yttrium Aluminum Garnet
ZND	Zeldovich, Von Neumann, Deering

A	Area or Pre-exponential Factor or Constant
B	Constant
C	Constant or Heat Capacity in the Theory of DDT Type Ignition
C_v	Heat Capacity at Constant Volume
C_p	Heat Capacity at Constant Pressure
C_V	Average Heat Capacity
D	Detonation Velocity
E	Energy or Energy Fluence in the Theory of SDT Type Ignition
E_a	Activation Energy
E_c	Critical Energy Fluence in the Theory of SDT Type Ignition
E_{ign}	Ignition Energy
F	Force or Fraction of Explosive that has reacted
G	Gibbs Free Energy or Growth Rate Function or Constant in the Lee-Tarver Ignition and Growth Model
G_a	Gibbs Free Energy of Activation
H_{fus}	Heat of Fusion
ΔH_v	Heat of Evaporation
ΔH_{sub}	Heat of Sublimation
ΔH	Enthalpy
I	Constant in the Ignition and Growth Theory or Light Intensity
L	Length or Characteristic Length in the Theory of Krause
P	Shock Pressure in the Theory of SDT
P_o	Initial Pressure
P_{cr}	Critical stress
P_1	Final State Pressure
$P(T)$	Radiation Term in the Theory of DDT Type Ignition
R	Gas Constant
R_1	Constant in the Lee-Tarver Ignition and Growth Model
R_2	Constant in the Lee-Tarver Ignition and Growth Model
S	Entropy of the System
T	Temperature

T_o	Initial Temperature
T_c	Critical Temperature in the Theory of DDT Type Ignition
$T_c^{'}$	Critical Temperature in the Theory of Hot Spots
T_d	Deflagration Temperature
T_1	Final State Temperature
T_m^0	Normal Melting Point
T_m	Melting Point
T_U	Ambient Temperature in the Theory of Krause
Q	Heat of Reaction or Heat of Decomposition in the Theory of DDT Type Ignition
U	Internal Energy of the System or Shock Velocity in the Theory of SDT Type Ignition
V_o	Specific Volume or Initial Specific Volume of Explosive
V_1	Final State Volume or Specific Volume of Shocked, Unreacted Explosive
W	Mass Fraction of Undecomposed Material
Z	Geometry Factor of the Burning Material or Collision Number in the Theory of DDT Type Ignition
a	Radius or Half-thickness in the Theory of DDT Type Ignition
a	Thermal Diffusivity in the Theory of Krause
c	Specific Heat
e	Internal Energy in the Conservation Laws or Emissivity in the Stefan-Boltzmann's law
h	Planck's Constant
k_0	Pre-exponential Factor
k_B	Boltzmann's Constant
m	Mass
n	Number of Moles
p	Pressure in the Lee-Tarver Ignition and Growth Model
p_s	Shock Pressure in the Theory of Hot Spots
p^z	Pressure Dependent Laminar Burn Rate
r	Constant in the Lee-Tarver Ignition and Growth Model

t	Time
u	Particle Velocity in the Theory of SDT
u_p	Particle Velocity
v	Specific Volume
w	Volume or Beam Radius in the Theory of DDT
x	Constant in the Lee-Tarver Ignition and Growth Model
y	Constant in the Lee-Tarver Ignition and Growth Model
z	Constant in the Lee-Tarver Ignition and Growth Model
α	Pressure Coefficient of Melting Point in the Theory of Hot Spots or Absorption Coefficient in the Theory of DDT Type Ignition
∇^2	Laplacian Operator
δ	Shape Factor in the Theory of DDT Type Ignition
δ_1, δ_2	Dimensionless Parameters in the Theory of Krause
Θ	Dimensionless Variable in the Theory of Krause
ϑ	Temperature Difference in the Theory of Krause
λ	Thermal Conductivity or Thermal Diffusivity in the Theory of DDT Type Ignition
λ^*	Degree of Chemical Reaction
ξ	Dimensionless Coordinate in the Theory of Krause
ρ	Density
ρ_o	Density of Unshocked Material
σ	Stefan's Constant
τ	Characteristic Time
ω	Grüneisen Coefficient

1. Introduction

Energetic materials are materials that have fuel and oxidizer in the same molecule or in an intimate mechanical mixture of several molecules and include both explosives and propellants. Useful energetic materials have chemical energy between 2900 and 6700 J/g.[1] A traditional way to initiate detonation in explosive material has been to use hot wire detonators or igniters. These devices of initiation are also known as electroexplosive devices. There are associated serious safety problems with them because of electromagnetic radiation and spurious electrical signals in many applications for example in space and military technology and also in blasting technology.

In today's blasting technology and in some military applications nonelectric detonators are used, where a hollow plastic shock tube delivers the firing impulse to the detonator, making it immune to hazards associated with stray electrical currents. The latest electronic initiation systems with digital detonators are also considered to be quite immune to the hazards associated with stray electrical currents.

Laser-initiated devices do not contain electrical circuits and are not directly attached to electrical equipment. Between the laser source and the individual explosive component, nonconductive fiber optics is used. This basic construction leads to better electrical immunity.[4] The safety and insensitivity demands for energetic materials and ignition systems in many applications recommend the use of laser-initiated devices.

The use of lasers as ignition sources has been extensively applied to studies of the ignitability of explosives and pyrotechnical materials. The laser was first introduced as an ignition source for energetic materials by Brish et al[2, 3] and Menichelli and Yang[4, 5] in the sixties and early seventies. They did the studies using a Q-Switched Ruby laser and a YAG-laser. The ignition mechanism is from

shock to detonation transition (STD). Laser ignition studies of both deflagration and detonation using a CO_2 laser have also been carried out. The ignition mechanism with explosives is from deflagration to detonation transition (DDT).

The diode laser is increasingly used as an ignition device for pyrotechnic mixtures or propellants and for explosives. When using this device, the ignition mechanism with explosives is also from deflagration to detonation transition.

To understand both ignition mechanisms – from deflagration to detonation and from shock to detonation – it is useful to know the basic theory of detonation and know the theoretical descriptions of ignition. Experimental laser ignition studies have proved to be very important for understanding the ignition mechanisms. One significant result of the experiments has been the discovery of a strong dependence between the energy necessary for ignition and the surrounding gas pressure. The conclusion that can be drawn is that the ignition process is not only a solid phase reaction but is a complex process where gas, liquid, and/or solid phase reactions are involved.

The technical evolution has taken place in laser sources - diode lasers and YAG lasers – making them increasingly economically viable for many applications of ignition devices and ignition systems. As a proof from this many published patents for defense and space applications can be mentioned and in conference presentations laser initiation devices and systems for both applications have been published.

2. Theory of burning and detonation

2.1 Burning

Burning or combustion is known as a complex sequence of exothermic chemical reactions between a fuel and an oxidant, which mostly consists in oxygen in the air. Many materials based on carbon and hydrogen compounds, including wood, burn indirectly so that the combustion takes place as a reaction between oxygen and the gases released from the material. An exception from this rule is the glowing combustion of charred wood where oxygen reacts directly with carbon. Under the influence of heat, wood easily produces substances that react eagerly with oxygen, leading to the high propensity of wood to ignite and burn.[6, 7]

Ignition and combustion of wood is mainly based on the pyrolysis, i.e. thermal decomposition of cellulose and lignin, and the reactions of pyrolysis products with each other and with gases in the air, mainly oxygen. When temperature increases and its level is high enough, about 270^{o}C, cellulose starts to pyrolyse. The decomposition products either remain inside the material or are released as gases. Gaseous substances react with each other and oxygen, releasing a large amount of heat that further induces pyrolysis and combustion reactions. Combustion reactions are accompanied many times by production of light in the form of either glow or flames.[6, 7]

Empirically it has been observed that the temperature dependence of the reaction rate follows the Arrhenius equation:[8]

$$k = Ae^{-E_a/RT}, \qquad (2.1.1)$$

where A is called the pre-exponential factor and will vary depending on the order of the reaction. E_a is the activation energy, R is the gas constant and T is the

temperature in Kelvin. In the Fig. 2.1 two reaction profiles are depicted schematically for reactants 1 and reactants 2. The horizontal axis is the reaction coordinate, and the vertical axis is the potential energy. The enthalpy in the exothermic reaction is ΔH. In the decomposition of an energetic material, the reaction can be written in the simplified form: $(ABC) \leftrightarrow (ABC)^{\#} \rightarrow A + B + C$, where $(ABC)^{\#}$ describes the activated complex.

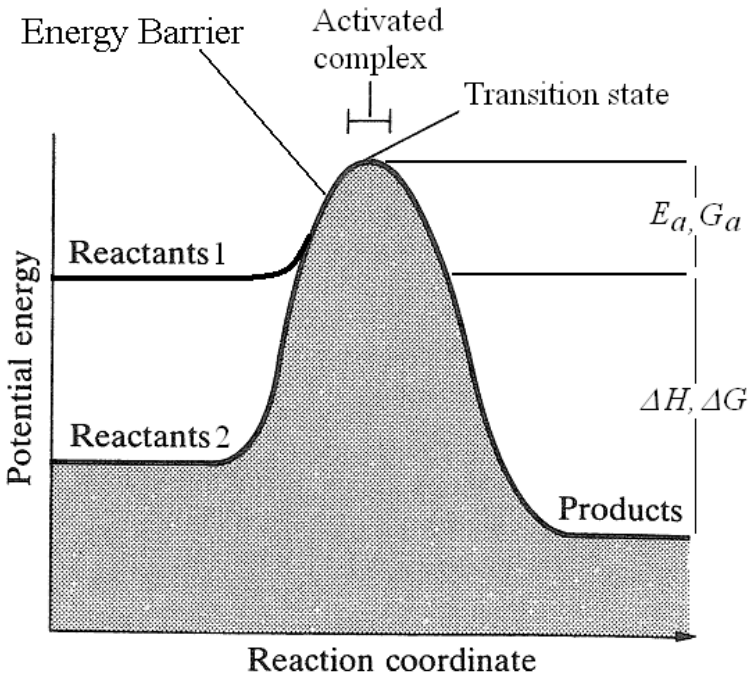

Fig. 2.1.1 The diagram of a reaction profile. The horizontal axis is the reaction coordinate, and the vertical axis is potential energy.

The transition state theory of chemical reactions gives for chemical reactions:[9]

$$k = \frac{k_B T}{h} e^{-\Delta G_a / RT}, \tag{2.1.2}$$

where G_a is Gibbs free energy of activation, k_B is Boltzmann's constant, and h is Planck's constant. In the transition state theory, an activated molecule is formed

during the reaction in the transition state between forming products and reactant or reactants. It is also known as the activated complex theory or the theory of absolute reaction rates.[8]

The Gibbs free energy has the form: $G = U + pV - TS$, where U is the internal energy of the system and S is the entropy of the system. The enthalpy of the system has the form: $H = U + pV$, which has a negative value in the case of exothermic reactions, for example, in the case of burning. In the constant pressure the system's enthalpy H, is decreased by the amount of $\Delta H < 0$. The free energy of activation includes an entropy term as well as an enthalpy term, both of which depend on temperature. In the Fig. 2.1.1 $\Delta G = \Delta H$ is the heat of the decomposition reaction of an explosive molecule, as an example.

The activation energy has been understood in quantum mechanics to be a potential energy barrier separating two minima of potential energy, of the reactants and of the products of reaction. When the temperature rises the molecule has a higher probability to penetrate the potential energy barrier.[8]

The precise form of the temperature dependence depends upon the reaction, and can be calculated using formulas from statistical mechanics involving the partition functions of the reactants and of the activated complex.[9]

The Arrhenius burning equation for energetic materials has the form:

$$W_j^{n+1} = W_j^n - \Delta t Z W_j^n e^{-E_a/RT_j^n}, \qquad (2.1.3)$$

where $1 \geq W \geq 0$. W is the mass fraction of undecomposed material. Z is 1 for slabs, 2 for cylinders and 3 for spheres. E_a is the activation energy. R is the gas constant and T is the temperature in Kelvins.[17]

2.2 Deflagration

Deflagration is a process of subsonic combustion that usually propagates through thermal conductivity; hot burning material heats the next layer of unburned material causing decomposition and oxidation. The process is propagating by releasing energy. In deflagration the linear speed of the reaction front is classified as being between 0.001 and 1500 ms^{-1}. Sometimes the slowly deflagration is classified as the reaction speed of 0.001 to 10 ms^{-1} and correspondingly fast deflagration is classified as the speed of 10 to 1500 ms^{-1}. In the Table 2.2.1 some typical qualities of combustion, deflagration and detonation are compared.

	Combusting Solid Fuel	Deflagrating Energetic Material	Detonating Energetic Material
Material or element and oxidant	Carbon and hydrogen with oxygen in air	Propellant, molecular structure usually includes the oxidant	High Explosive, molecular structure includes the oxidant
Linear speed of the reaction front [m/s]	10^{-5}	$1x10^{-3} – 1.5x10^{3}$	$2x10^{3}$ - $9x10^{3}$
The character of the chemical reaction	Redox mechanism	Redox mechanism	Redox mechanism
Reaction time [s]	10^{-1}	10^{-3}	10^{-6}
Propagation of the reaction	Heat conduction	Heat conduction	Shock front and phonon flow
Heat of reaction [kJ/kg]	10^{4}	10^{3}	10^{3}
Power [W/cm^{3}]	10	10^{3}	10^{9}
Typical mechanism of ignition	Heat	Hot particles, hot gases, hot spots	High temperature with confinement, shock wave, hot spots
Typical overpressure following the reaction front [bar]	0 – 7	$7 – 7x10^{3}$	$70 – 7x10^{5}$

Table 2.2.1 Comparison between some typical properties of combustion, deflagration and detonation.

Deflagration is a typical way of burning in the case of powders and pyrotechnical materials. A powder is usually stoichiometric mixture of oxidant and fuel. It may be a mixture of several materials, for example black powder or it may be a

composite propellant consisting of oxygen-donating inorganic salts and a binder made of plastic or nitrates and perchlorates and plastic binders. Ammonium Perchlorate (AD) in particular is used as an oxidizer. RDX or other similar energetic materials are used as nitrates. It may be nitrated hydrocarbons, such as cellulose nitrate powders.[10]

Sometimes black powder is classified as a pyrotechnical material. Other typical pyrotechnical materials are smoke producing mixtures and color light producing mixtures.

Under certain circumstances and conditions, a burning or deflagration reaction can grow into a full steady-state detonation. If an explosive is ignited, it starts to deflagrate, and if it is confined so that the reaction product gases cannot escape, then the gas pressure in the deflagrating region builds up. Burning reaction rates are a function of pressure as well as temperature and therefore the reaction rate increases as pressure increases.[14]

2.3 Detonation

Detonation is a supersonic form of combustion. It proceeds through the explosive as a wave, traveling at several times the speed of sound in the material. Detonation differs from other forms in that all the important energy transfer is by mass flow in strong compression waves, with negligible contributions from other processes like heat conduction which are so important in flames. The shock heats the material by compressing it, thus triggering chemical reaction, and a balance is attained so that the chemical reaction supports the shock. The material is consumed 10^3 to 10^8 times faster than in a flame, making detonation easily distinguishable from other combustion processes. Wave velocities in solid and liquid explosives have a range from 2000 to 9000 m/s. For example, the

detonation wave in RDX with an initial density of 1.76 g/cm^3 travels 8750 m/s.[10, 12]

In the detonation theory, the detonation is seen as a shock wave moving through an explosive. The thermodynamic state of the system is accurately described by the Chapman-Jouguet model (C-J model).[11, 12] This theory does not provide insight into the molecular level events occurring in the solid behind the shock front. These are the zones which lie between the unreacted solid and the reaction products.[13] The broader theory is known as ZND-model (Zeldovich, Von Neumann, Deering, in the early 1940s). The basic assumptions in this theory are[14]: 1. The flow is one dimensional. 2. The front of the detonation is a jump discontinuity. 3. The reaction-product gases leaving the detonation front are in chemical and thermodynamic equilibrium and the reaction is completed. 4. The chemical reaction-zone length is zero. 5. The detonation rate or velocity is constant. 6. The gaseous reaction products, after leaving the detonation front, may be time dependent and are affected by the surrounding system or boundary conditions.

The assumption 2 neglects the transport effects: Heat conduction, Radiation, Diffusion and Viscosity. The assumptions 3, 4, 5 and 6 can be written in other words: 3b. The reaction rate is zero ahead of the shock and finite behind, and the reaction is irreversible[12]. It proceeds in the forward direction only. 4b. All thermodynamic variables other than the chemical composition are in local thermodynamic equilibrium everywhere[12].

With these constraints, the detonation is seen as a shock wave moving through an explosive. The shock front compresses and heats the explosive, which initiates a chemical reaction. The exothermic reaction is completed instantly. The energy liberated by the reaction feeds the shock front and drives it forward. At the same time the gaseous products behind this shock wave are expanding and a rarefaction moves forward into the shock. The shock front, the chemical reaction, and the

leading edge of the rarefaction are all in equilibrium. They are all moving at the same speed, which is the detonation velocity D.[14]

In the Figure 2.3.1 (a) is depicted as an idealized shock front propagating through a material. The initial state is characterized by a pressure P_o, a temperature T_o, and a specific volume V_o. The final state is characterized by P_1, T_1, and V_1. The front of the shock does not change shape over time, which means that the pressure remains constant over time. The detonation velocity does not change over time.

Figure 2.3.1 (b) shows the essential physical and chemical elements of the shock wave in the detonation. The shock front has a finite rise time. Typically the rise of the front extends over a few nm, corresponding to a rise time of ~1 ps.[11, 12]

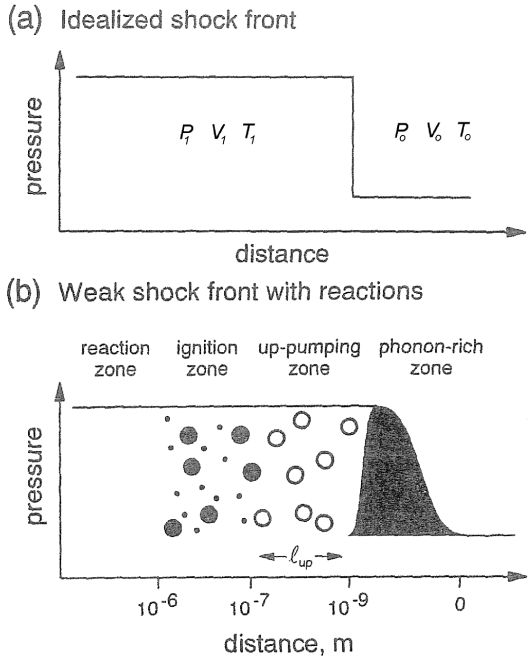

Fig. 2.3.1 The idealized shock front a) and the weak shock front with reaction zones b). The breadth of the up-pumping zone is l_{up}.[15]

In **the phonon rich zone** the molecular vibrations, which are not directly pumped by the shock, have yet to be excited. In **the up-pumping zone**, the energy in the phonon modes is transferred to the vibrations by multiphonon up-pumping process. These two baths equilibrate within ~10^{-10} s corresponding to 10^{-7} m. As the vibrational modes are excited, reactivity is enhanced and bond breaking due to thermal decomposition occurs in the molecules. This is **the ignition zone** and extends to ~10^{-9} s and 10^{-6} m behind the shock front. In explosives and other energetic materials, endothermic bond breaking reactions are the precursors to detonation, a series of exothermic chain reactions occurring in **the reaction zone** 10^{-8} - 10^{-6} s corresponding to 10^{-5} -10^{-3} m behind the front.[16, 17]

In the Figure 2.3.2 depicts a *P*-*V* plane representation of detonation. *P* is the pressure and *V* is the specific volume. The density is ρ, which is the inverse value of the specific volume, $V = 1/\rho$. The point (A) represents the initial state of the unreacted explosive. At the point (A) the explosive is in the pressure of P_o. This pressure P_o may usually be 1 bar. The explosive has a specific volume of V_0. The initial density is ρ_0. The state at the point (C) indicates the jump condition to the fully shocked but as yet unreacted explosive. In Figure 2.3.1 that means just the jump from the pressure P_o to P_1. On the other Hugoniot, the point (B) represents the state of reaction products.

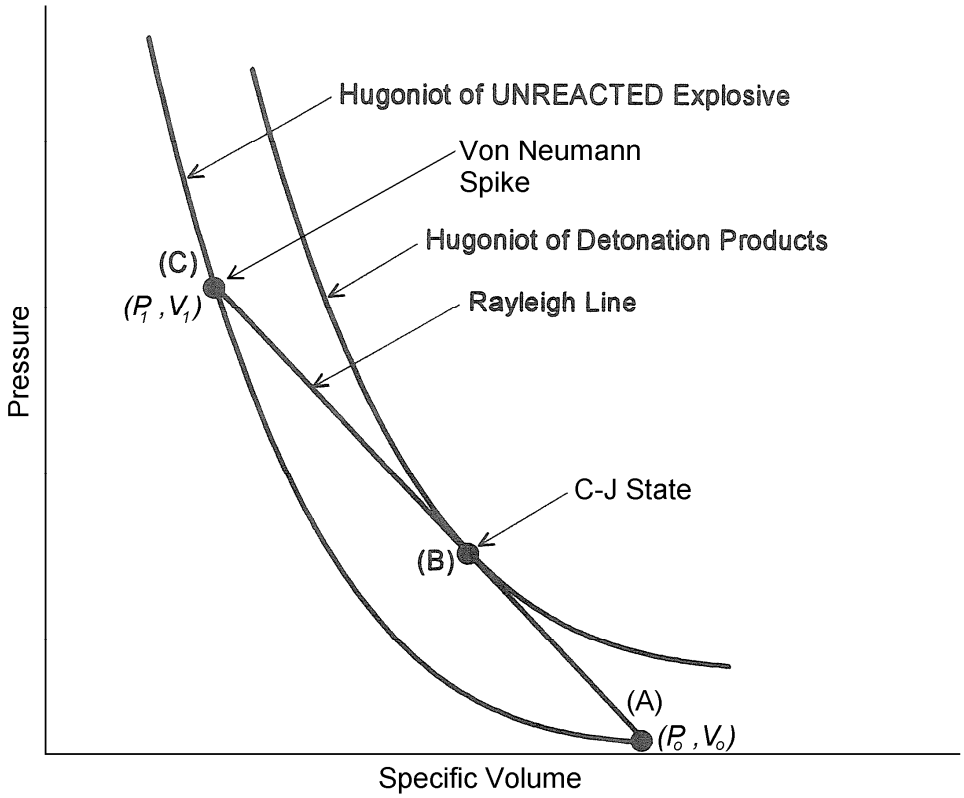

Fig. 2.3.2 *P*-*V* plane representation of detonation with the Hugoniot curves of unreacted explosive and detonation products.[14]

The line from the point (A) through the point (B) to the point (C) is called the Raleigh Line. The state of reaction products is at the point where the Raleigh line tangent to the products Hugoniot at the point (B). This is called the Chapman-Jouguet C-J state (Figure 2.3.2).

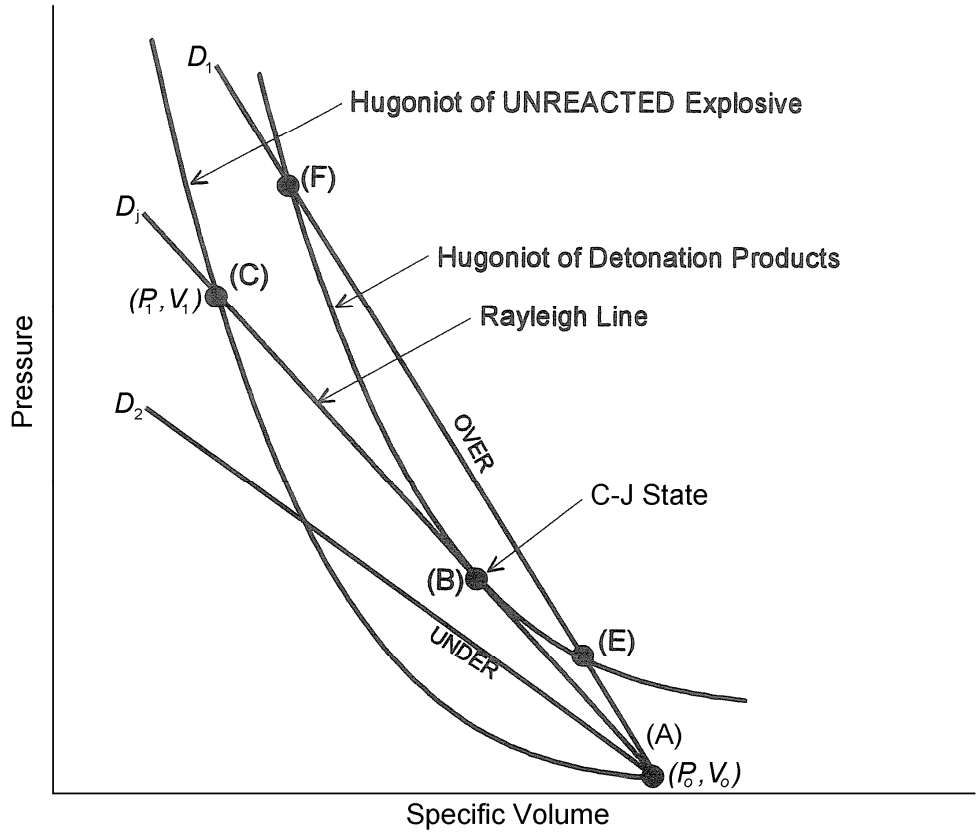

Fig. 2.3.3 Various Raleigh line possibilities.

The conservation conditions require that the final state point in the *P*-*V* plane lie on both the Hugoniot curve of detonation products and the Rayleigh line.

Three of the possible Raleigh lines (Eq. (2.3.2.3)) are depicted in Fig. 2.3.3. Each of them represents a different value of detonation velocity, say D_1 (OVER), D_j and D_2 (UNDER). For a sufficiently small value of detonation velocity D_2 the Raleigh line and the Hugoniot curve of detonation products have no intersection, so there is no solution that satisfies the assumption (2.3.9). For a large detonation velocity value, say D_1, there will be two solutions which are marked *F* (strong) and *E* (weak) in the figure. The flow at the point *F* or at the strong point is supersonic with respect to the detonation front, and a disturbance arising behind the front will overtake it. At the point *E* or at the weak point the flow is subsonic with respect to

the detonation front, and a disturbance behind the front will fall farther behind. At the tangent point, the C-J state, the flow is sonic.[12,14]

In the case of a concave shock front, as in an implosion, the convergence effects may raise the pressure well above the C-J state, with a corresponding increase in the detonation velocity D.[17]

Figure 2.3.4 depicts the pressure variation as a function of distance when a detonation wave moves through the explosive. The scale is larger than in the picture (2.3.1) (a) and especially much larger than in the picture (2.3.1) (b). In the initial step of a popular and much used explanation for the initiation of detonation the shock wave created by the booster or by some other way hits the surface of the explosive, which compresses. The temperature rises above the ignition point of the material, initiating chemical reaction within a small region just behind the shock wave. This small region is known as the reaction zone. Detonation occurs when the reaction propagates through the explosive at shock velocity. The rapid rise in pressure is what brings on the reaction. This is known as the Von Neuman spike. The C-J state (Chapman-Jouguet state) represents the state of the detonation products at the end of the reaction zone. The gas expansion is described using the equation of state developed by Taylor. The gas expansion wave is called as the Taylor wave (Figure 2.3.4). In the case of unreacted explosive, the pressure is $P = P_o$ and the particle velocity is $u = 0$. In the C-J state the pressure is P_{CJ}.

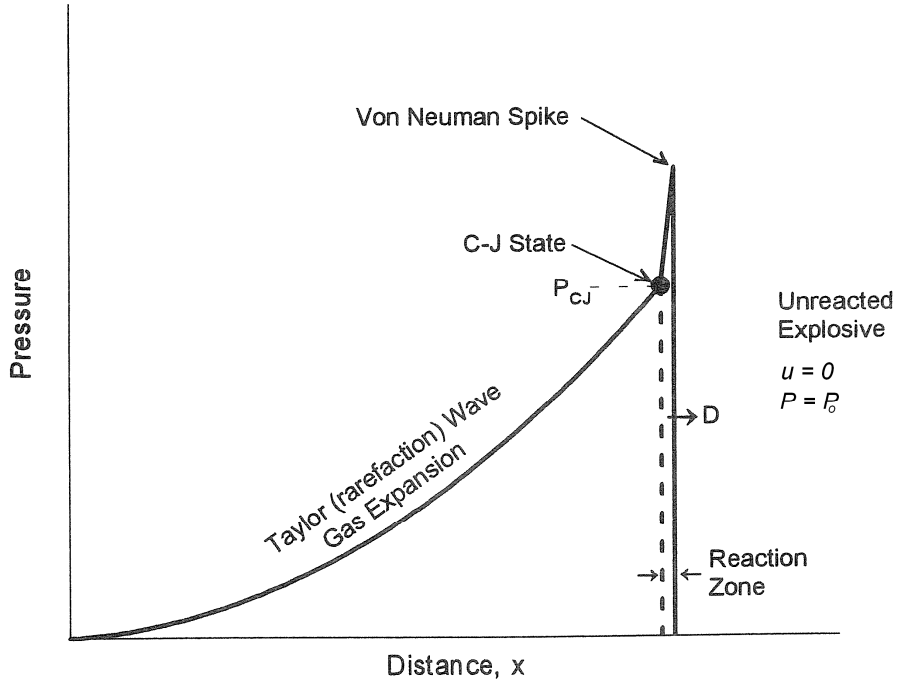

Fig 2.3.4 Pressure vs distance diagram of a detonation wave.[14]

If the explosive has heavy rear and side confinement, the gases cannot expand as freely as unconfined gases; thus the Taylor wave is higher and longer as is depicted in Figure 2.3.5. When the explosive is very thick along the detonation axis, the Taylor wave is higher. When the explosive is very thin and there is little rear or side confinement, the Taylor wave is lower. The actual shape of the Taylor wave is governed then by a combination of the isentrope for expansion of the detonation gases, the charge size, and the degree of confinement.[14]

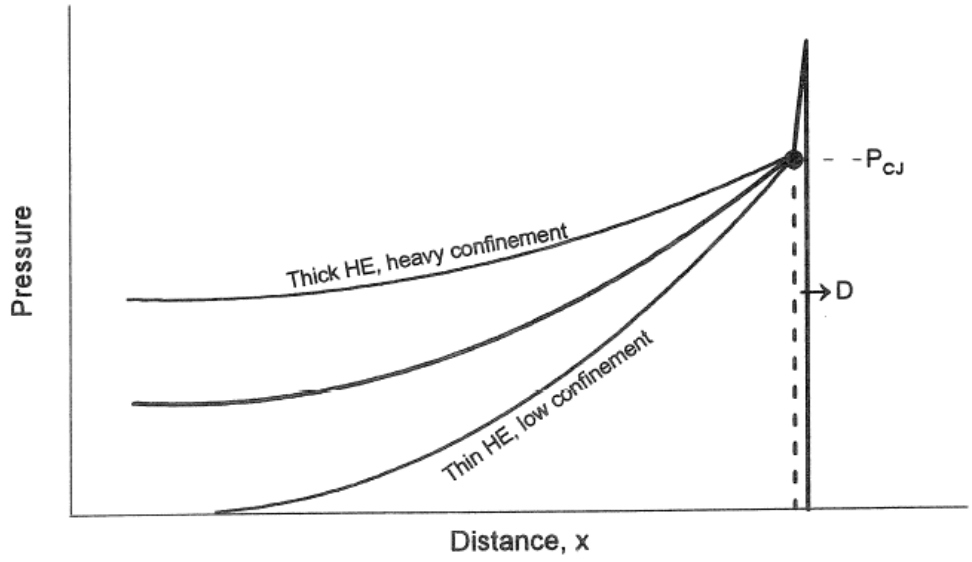

Fig 2.3.5 The influence of confinement on the Taylor wave in the case of thick High Explosive and in the case of thin High Explosive.[14]

In the case of laser ignition heavy rear and side confinement was created using the mechanical environment of the laser ignition pellet (see Figure 4.1.2) and with the static high pressure of the gas in the ignition chamber.

Before writing the Hugoniot equation on the P-V plane or the equation of state of high explosive the conservation laws have to be proved.

2.3.1 Conservation of Mass[12, 14, 17]

Figure 2.3.6 depicts a cylindrical material volume passing through a shock front. The parameters in front of the shock-wave (Shock Front) are: Particle velocity u_0, density ρ_0, internal energy E_0, and pressure P_0. The parameters behind the shock-wave suddenly change across the shock front and are: Particle velocity u_1,

density ρ_1, internal energy E_1, and pressure P_1. The relative velocity of the material is *D*. If the case is the detonation of energetic material, *D* represents the detonation velocity. When the material is standing still before it is detonated or shocked, the particle velocity u_0 is equal to zero, $u_0 = 0$.

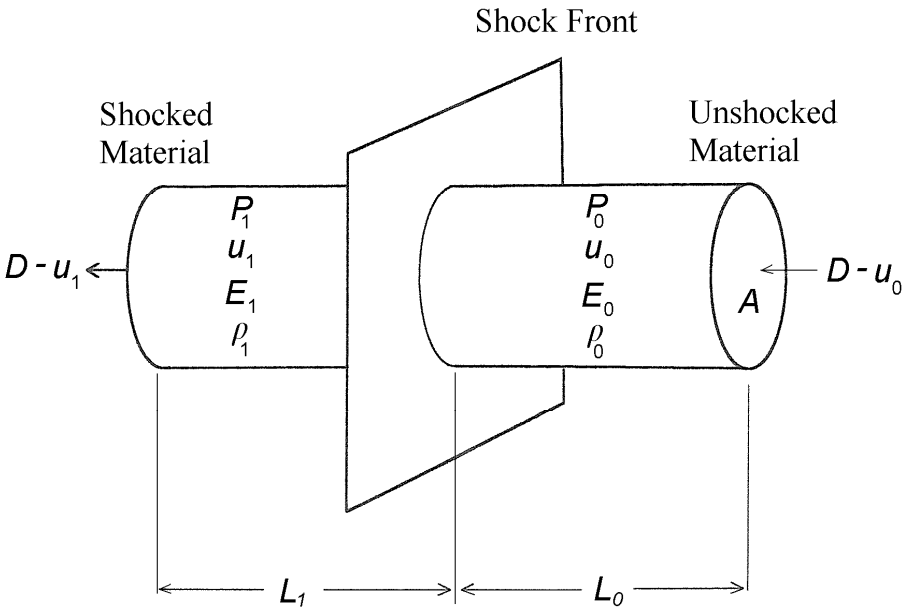

Fig 2.3.6 Material is passing through a shock front. The velocity of the material is *D*. The cross-sectional area of the material is *A*.[14]

The conservation of mass implies that the mass entering equals the mass leaving. Mass *m* is equal to density ρ times volume V: $m = \rho V$. When the volume V is equal to the area *A* times length *L*: $V = AL$.

Length in a system like that in Fig 2.3.6 can be found as the distance a particle travels relative to the shock front, which is the velocity relative to the front times the time it took travel that length: $L = t \times velocity(relative) = t(D - u)$.

The mass entering is: $m = \rho_0 V_0$ and the mass leaving is: $m = \rho_1 V_1$. Thus: $m = \rho_0 A L_0$ and $m = \rho_1 A L_1$. On the other hand, using the equation of the length *L* is: $m = \rho_0 A t (D - u_0)$ and $m = \rho_1 A t (D - u_1)$. The mass in is equal to the mass out and thus: $\rho_0 A t (D - u_0) = \rho_1 A t (D - u_1)$ or $\rho_0 (D - u_0) = \rho_1 (D - u_1)$, which is the mass equation. It can be written as:

$$\frac{\rho_1}{\rho_0} = \frac{D - u_0}{D - u_1} \qquad (2.3.1.1)$$

In most cases, as mentioned before: $u_0 = 0$ and thus:

$$\frac{\rho_1}{\rho_0} = \frac{D}{D - u_1} \quad \text{or} \quad \rho_0 D = \rho_1 (D - u). \qquad (2.3.1.2)$$

Density can be represented by the reciprocal of specific volume v: $v = 1/\rho$ and the mass equation (2.3.1.1) can be written in the form:

$$\frac{v_0}{v_1} = \frac{D - u_0}{D - u_1} \qquad (2.3.1.3)$$

2.3.2 Conservation of Momentum[12, 14, 17]

The conservation of momentum implies that the rate of change in momentum, for the mass (Fig. 2.3.6) to go from the state before the shock to the state after the shock, must be equal to the force applied to it. The force applied is simply the pressure difference across the front times the area over which it is applied, the material cross-sectional area: $F = (P_1 - P_0) A$. The rate of change in momentum

is: $rate = (mu_1 - mu_0)/t$. Deriving the mass-balance equation gives $m = \rho At(D-u)$ and thus: $rate = \left[\rho_1 Atu_1(D-u_1) - \rho_0 Atu_0(D-u_0)\right]/t$. Canceling *t* out of this equation and equating this to the equation of *F* above gives: $(P_1 - P_0)A = \rho_1 Au_1(D-u_1) - \rho_0 Au_0(D-u_0)$ and canceling out *A* leaves: $(P_1 - P_0) = \rho_1 u_1(D-u_1) - \rho_0 u_0(D-u_0)$. The mass equation (2.3.1.1) gives: $\rho_1(D-u_1) = \rho_0(D-u_0)$. Combining these two equations yields:

$$P_1 - P_0 = \rho_0(u_1 - u_0)(D-u_0), \qquad (2.3.2.1)$$

which is the momentum equation. The common case, where $u_0 = 0$ gives:

$$P_1 - P_0 = \rho_0 u_1 D. \qquad (2.3.2.2)$$

When u_1 is eliminated from the conservation equation of mass and momentum the result defines the Rayleigh line (Fig. 2.3.3), which is expressed by:

$$\rho_0^2 D^2 - \left(P - P_0\right)/\left(v_0 - v\right) = 0. \qquad (2.3.2.3)$$

2.3.3 Conservation of Energy[12, 14, 17]

The conservation of energy implies that the rate of energy increase of the mass (Fig 2.3.6) is equal to the rate of work being done on it. The rate of work done on the mass would be the change in the pressure-volume product divided by the time required for the process. The volume divided by time is the same as area times velocity, thus the rate at which work is done on the mass is: $w/t = P_1 Au_1 - P_0 Au_0$. The rate of energy increase of the mass is the sum of the rate of change in internal energy plus the rate of change in kinetic energy. The internal energy, *E*, is the mass times the specific internal energy, *e*:

$E = me = \rho ALe$, and the rate of change in internal energy is: $E/t = (\rho_1 AL_1 e_1 - \rho_0 AL_0 e_0)/t$. The rate of change in kinetic energy is: $E_{kin}/t = (½\rho_1 AL_1 u_1^2 - ½\rho_0 AL_0 u_0^2)/t$. Repeating the above, the rate of work done is equal to the rate of change in energy, and therefore, $P_1 Au_1 - P_0 Au_0 = (\rho_1 AL_1 e_1 - \rho_0 AL_0 e_0)/t + (½\rho_1 AL_1 u_1^2 - ½\rho_0 AL_0 u_0^2)/t$.

Substituting in this the expression of L, $L = t(D-u)$, which is derived in the chapter on conservation of mass (2.3.1), and canceling the A gives: $P_1 u_1 - P_0 u_0 = \rho_1 (D-u_1)(e_1 + ½u_1^2) - \rho_0 (D-u_0)(e_0 + ½u_0^2)$. Considering from the chapter on conservation of mass that $\rho_0 (D-u_0) = \rho_1 (D-u_1)$ gives the energy equation or the equation of conservation of energy:

$$e_1 - e_0 = \frac{P_1 u_1 - P_0 u_0}{\rho_0 (D-u_0)} - ½(u_1^2 - u_0^2). \qquad (2.3.3.1)$$

In the common case where $u_0 = 0$ and considering the equation of mass (2.3.1.2) $\frac{\rho_1}{\rho_0} = \frac{D}{D-u_1} = \frac{v_0}{v_1}$ and the equation of momentum (2.3.2.2) $P_1 - P_0 = \rho_0 u_1 D$ gives:

$$e_1 - e_0 = ½(P_1 + P_0)(v_0 - v_1). \qquad (2.3.3.2)$$

Considering the explicit assumptions of the ZND model and applying the laws of conservation of mass and momentum to the shock front (Fig 2.3.1 (a)) gives the mass equation, the momentum equation and the energy equation:

$$\frac{V_1}{V_0} = \frac{\rho_0}{\rho_1} = \frac{D-u_1}{D-u_0}, \qquad (2.3.1)$$

$$P_1 - P_0 = \rho_0 (D-u_0)(u_1 - u_0), \qquad (2.3.2)$$

$$e_1 - e_0 = \frac{P_1 u_1 - P_0 u_0}{\rho_0 (D - u_0)} - \frac{1}{2}(u_1^2 - u_0^2), \qquad (2.3.3)$$

where the subscripts 0 and 1 refer to the states just in front of and just behind the shock front, respectively. *D* is the shock velocity (= detonation velocity) and *u* is the particle velocity. e_0 is the specific internal energy of the solid explosive at (P_0, V_0). e_1 is the specific internal energy of the reaction products at (P_1, V_1). The equation (2.3.1) is the mass equation, the equation (2.3.2) is the momentum equation and the equation (2.3.3) is the energy equation. A derivation of these conservation equations is presented for example in references [5] and [7]. In the common case where $u_0 = 0$, these equations have the formula:

$$\frac{V_1}{V_0} = \frac{\rho_0}{\rho_1} = \frac{D - u_1}{D}, \qquad (2.3.4)$$

$$P_1 - P_0 = \rho_0 u_1 D, \qquad (2.3.5)$$

$$e_1 - e_0 = \frac{1}{2}(P_1 + P_0)(V_0 - V_1). \qquad (2.3.6)$$

The energy equation (2.3.6) is known as the Hugoniot equation on the *P*-*V* plane (Figure 2.3.2). It has been commonly called the equation of state of high explosive but, according to some references[17] this is misleading.

According to the simple theory of detonation[12] the Hugoniot equation is proved beginning from the equation of state of polytropic gas (ideal gas with constant heat capacity). The equation of state of an ideal gas is: $PV = nRT$, where *n* is the number of moles of the gas. In the case of a polytropic gas with reaction $A \rightarrow B$ having constant enthalpy of complete reaction ($-\Delta H = q$) the equation of state is:

$$pv = RT \tag{2.3.7}$$

and the specific internal energy is:

$$e = C_v - \lambda^* q = pv(\gamma - 1) - \lambda^* q\,, \tag{2.3.8}$$

where C_v is the constant-volume heat capacity and λ^* specifies the degree of chemical reaction, changing from 0 for no reaction to 1 for complete reaction. The heat capacity for the ideal gas is equal: $\gamma = C_p / C_v$, where C_p is heat capacity at constant pressure. The Hugoniot curve is:

$$\left(\frac{p}{p_0} + \mu^2\right)\left(\frac{v}{v_0} + \mu^2\right) = 1 - \mu^4 + 2\mu^2 \frac{q}{p_0 v_0}\,, \tag{2.3.9}$$

where $\mu^2 = (\gamma - 1)/(\gamma + 1)$, p is the specific pressure and v is the specific volume.

There are three equations ((2.3.4), (2.3.5), and (2.3.6)) and five variables. Some numerical modeling methods for these have been developed. One of them is the widely used is BKW method based on the equation of state of Becker-Kistiakowsky-Wilson[17]. An extensive and thorough fundamental description of the BKW equation of state and method has been published in reference[17]. Many applications of the BKW model and method have been published and described in reference[17].

Figure (2.3.7) was plotted using the Fortran BKW computer program at the PVTT, calculating the Hugoniot curve for RDX, when the densities were 1.50, 1.65 and 1.80 g/cm^3. The BKW calculated parameters for RDX are published in Table (2.3.1). According to those results the CJ pressure and the detonation velocity increase, and, correspondingly, the CJ temperature and the CJ volume decrease, when the density of the RDX increases.

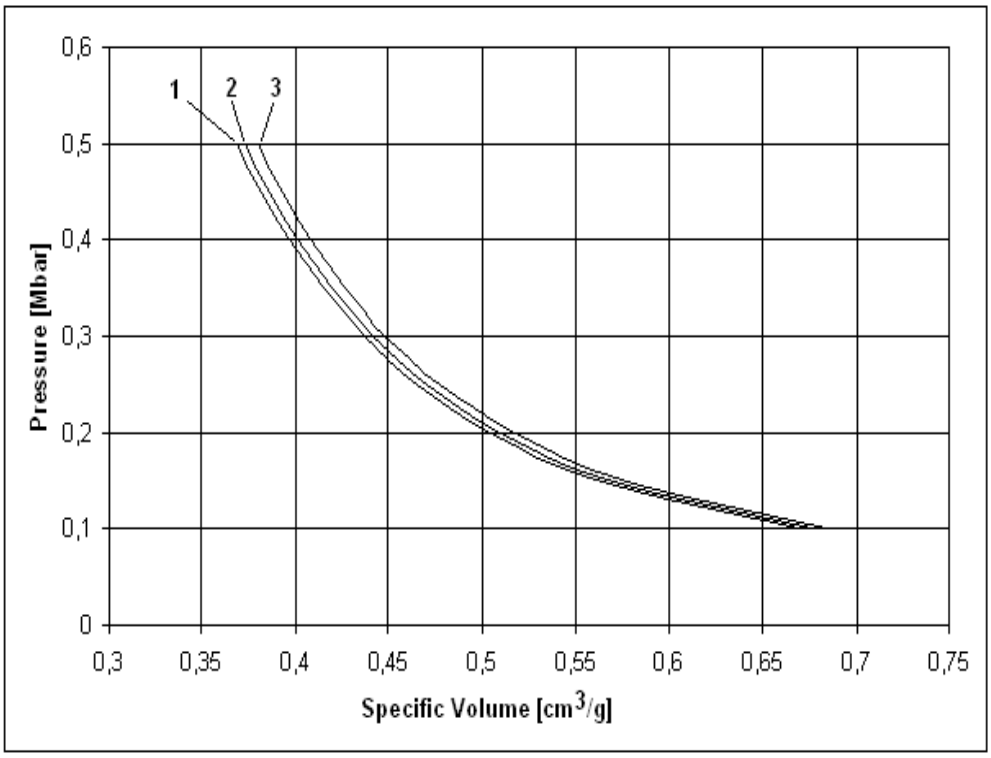

Fig 2.3.7 BKW calculated Hugoniot's for the reaction products of RDX when density is 1) 1.80 2) 1.65 and 3) 1.50.

Density of RDX [g/cm^3]	**1.50**	**1.65**	**1.80**
CJ Pressure [Mbar]	0.23037	0.28294	0.34666
Detonation Velocity [km/s]	7643.86	8176.88	8753.99
CJ Temperature [^{o}K]	3132.5	2880.1	2587.6
CJ Volume [cm^3/g]	0.49143	0.45062	0.41593
Computed γ	2.80437	2.89906	2.97904
Volume of the gas [cm^3/mole]	0.13600	0.12557	0.16223

Table 2.3.1 Some BKW calculated parameters for RDX when density is 1.50, 1.65 and 1.80.

2.4 Forest Fire Model

The basic mechanism of heterogeneous explosive shock initiation is shock interaction at density discontinuities, which produces local hot spots that decompose and add their energy to the flow[17]. Typical heterogeneous explosives are for example plastic bonded explosives.

According to the experimental studies with heterogeneous explosives a shock wave interacts with the density discontinuities, producing numerous local hot spots that explode but do not propagate. The released energy strengthens the shock, it interacts with additional inhomogeneities, higher temperature hot spots are formed and more of the explosive is decomposed. The shock wave grows

stronger, releasing more and more energy, until it becomes strong enough to produce propagating detonation.[18]

A model, called Forest Fire Model after its originator, Charles Forest,[19] has been developed for describing the decomposition rates as a function of the experimentally measured distance of run of detonation vs. shock pressure and the reactive and nonreactive Hugoniot. The model can be used to describe the decomposition from shocks formed either by external drivers or by internal pressure gradients formed by the propagation of a burning front for the heterogeneous explosives.[17]

A model for the burning resulting from the shock initiation of heterogeneous explosives is included by calculating the rate from the equation:[17]

$$W_j^{n+1} = W_j^n \left(1 - \Delta t e^{A+BP+CP^2+\ldots+XP^n}\right), \tag{2.4.1}$$

where

$$-(1/W)(dW/dt) = e^{A+BP+CP^2+\ldots+XP^n} \tag{2.4.2}$$

from $P_{minimum}$ to P_{CJ}. Here W is the mass fraction of undecomposed explosive and P is pressure in [Mbar]. A, B and C … are pre-calculated constants from tables of equation-of-state for some explosive. In equation (2.4.2): $(1/W)(dW/dt) = 0$ if $P < P_{minimum}$, and $W_j^{n+1} = 0$ if $P > P_{CJ}$ or $W_j^n < 0.05$.[17]

The Forest Fire rate model of shock initiation of heterogeneous explosives has been used to study the sensitivity of explosives to shock. The minimum priming charge test, the gap test, the shotgun test, sympathetic detonation, and jet initiation have been modeled numerically using the Forest Fire model.[20]

An extensive and thorough fundamental description of the Forest Fire model has been published in references[17, 19]. Some applications of the Forest Fire model are described in references[21, 22, 23, 24].

2.5 Hot spots

A hot spot is a localized region of higher-than-average temperature.[25] The relation between initiation of explosives and hot spots has been investigated by many researchers.[26, 27] The possible generation mechanisms of hot spots are:

1) Adiabatic heating of compressed gas spaces [28, 29],

2) A frictional hot spot on the confining surface or on a grit particle [28, 29],

3) Intercrystalline friction of the explosive itself [28, 29],

4) Viscous heating of explosive at high rates of shear [28],

5) Heating of a sharp point when it is deformed plastically [29],

6) Mutual reinforcement of relatively weak shock waves; probably at inhomogeneities in the shocked medium [30, 31, 32, 33],

7) Stagnation of particles spalled off a crystallite by incoming shock and then stopped after flying across an air gap by a neighboring crystallite (the cap can be a void) [34],

8) Micro-Munro jets formed by shocking bubbles, cavities or voids whose interface between solid or liquid and the cavity is concave [30].

Modes 1), 2), and 3) from these generation mechanisms operate most probably in the usual impact and/or friction initiation of pressed solid explosives whereas in the impact and/or friction initiation of liquid explosives only modes 1) and 2) operate. Modes 5), 6), 7), and 8) operate in the shock initiation and possibly the propagation of detonation in solid explosive compacts or explosive liquids containing inhomogeneities. Mode 4) is operative only at strong shock inputs and may be the main mode of initiation and propagation in homogeneous explosive liquids or defect-free explosive single crystals.[25]

In some references cases 1) to 5) are mentioned only as the generation mechanisms of hot spots.[14] The studies by some researchers indicate that these mechanisms would not produce sufficiently high temperatures. They proposed that the heart of the matter is the microjetting in bubbles and particle interstices and/or inelastic compression of solid particles.[35, 36] According to some references, a more believable mechanism is the inelastic flow of the solid explosives under impact, which produces the required temperatures.[37] The local areas are at high stress or pressure, and the melting point T_m is raised according to the formula [14]:

$$T_m = T_m^0 + \alpha P, \qquad (2.5.1)$$

where T_m^0 is the normal melting point at 1 atm, α is the melting point pressure coefficient and P is the pressure. For most CHNO explosives α is approximately 0.02°C/atm.[14]

Energetic material	T_m^0	T_d**[°C]**	**Heat of fusion [kJ/kg] ***)**
TNT	80.65-80.85 *)	290 **)	96.6
RDX	202 ***)	230 **) ***)	161
HMX	276-277 *)	270 **)	-
PETN	141.3 *) ***)	205 **) ***)	152
Tetryl	128.5-128.8 *)	190 **)	80

Table 2.5.1 The normal melting point T_m^0, the deflagration temperature T_d and heat of fusion of some energetic materials *) [38], **) [39], ***) [40].

In the case of from deflagration to detonation (DDT) type laser ignition measurements of RDX98/1/1 using the pressure of 50 bar, the melting point is raised by 1°C according to the equation (2.5.1).

The basic equation governing hot spot phenomena is [25]:

$$c\rho\frac{\partial T}{\partial t} = Qk_0 \exp(-E_a / RT) + \lambda\left(\frac{\partial^2 T}{\partial x^2} + \frac{n}{x}\frac{\partial T}{\partial x}\right) \qquad (2.5.2)$$

where $0 \le x < \infty$ and $t \ge 0$ with conditions: $t = 0$, when $T = T_o$, with the values $x < r$ and $T = T_1$, with the values $x > r$, $T_o > T_1$. When $t \ge 0$, and $x = 0$, $\partial T/\partial x = 0$, and when $x = \infty$, $\partial T/\partial x = 0$. In the equation (2.5.2): T is the temperature in Kelvin, x is the space coordinate, T_o is the initial hot spot temperature, T_1 is the medium temperature, Q is the heat of reaction, E_a is the activation energy, k_0 is the pre-exponential factor, c is the specific heat, λ is the thermal conductivity coefficient, ρ is the density and n is the hot spot symmetry factor. For the planar hot spot $n = 0$, for the cylindrical hot spot $n = 1$ and for the spherical hot spot $n = 2$. The exact solution of Equation (2.5.2) is unknown. Only numerical or approximate analytical solutions are available.

In a similar manner to the critical temperature T_c, the equation (2.5.1), defines the critical temperature $T_c^{'}$:[41]

$$P_{cr} = (T_c^{'} - T_m)/\alpha . \qquad (2.5.3)$$

The critical temperature $T_c^{'}$ is not been calculated for an infinite time to explosion, but for a time less than 10^{-5} s, which is the ignition delay time derived from observations in impact-machine experiments.[14]

Thus according to equation (2.5.3), the higher the local pressure, the higher the melting point, and the lower the critical stress to produce ignition. For most explosives the critical temperatures, $T_c^{'}$, is found to be between 400 and 600^{o}C;

hence the critical stress P_{cr} = 1x10^4 to 2.5x10^4 atm. The critical diameter of a hot spot is between 10^{-4} and 10^{-2} mm [41].

An empirical hot spot model in the case of shock wave initiation of heterogeneous explosive is described fundamentally in reference[42]. The general picture of shock initiation is shown schematically in Fig 2.5.1.. λ' specifies the degree of chemical reaction $0 \le \lambda' \le 1$, (0 for no reaction and 1 for complete reaction), τ_1, τ_2 and τ_3 are characteristic times for the process of hot spot formation, reaction, and growth, respectively, p is current pressure and p_s is shock pressure, $G(p, p_s)$ is the growth rate function.[42]

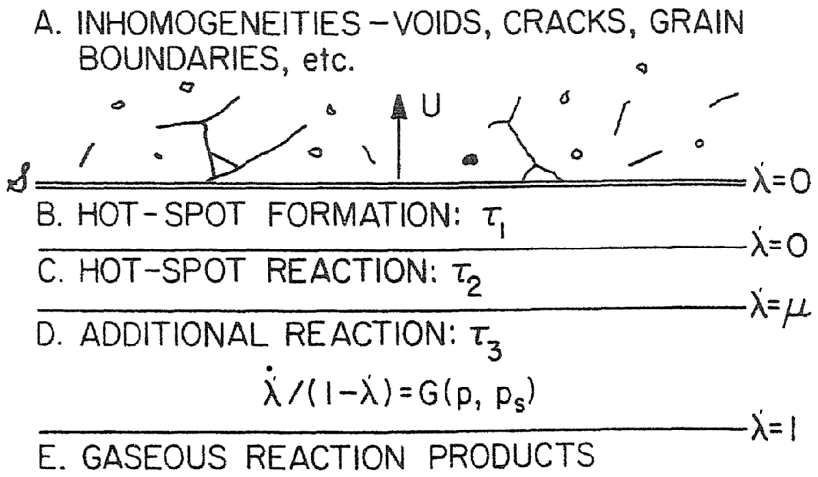

Fig 2.5.1 Schematic diagram of the multiple interacting processes in the phenomenological hot spot model. The steps B, C, D, and E are shown as independent processes when they, in fact, occur simultaneously.[42]

2.6 Lee-Tarver Ignition and Growth Model

A model of shock initiation in heterogeneous and homogenous explosives was developed in the late seventies by E. L. Lee and C. M. Tarver. It is called the "Lee-Tarver Ignition and Growth Model", "Ignition and Growth Model" or "Ignition and Growth reactive flow model".[43] The Ignition and Growth reactive flow model uses two Jones-Wilkins-Lee (JWL) equations of state[44], one for the unreacted explosive and another one for the reaction products. This equation of state has in the temperature-dependent form:

$$p = A \cdot e^{-R_1 V} + B \cdot e^{-R_2 V} + \omega C_V T/V , \qquad (2.6.1)$$

where p is pressure, V is relative volume, T is temperature, ω is the Grüneisen coefficient, C_V is the average heat capacity, and A, B, R_1 and R_2 are constants.

The chemical energy release rate laws in the ignition and growth models are based on considerable experimental evidence that the ignition of the explosive occurs in localized hot spots and that buildup to detonation occurs as the reaction grows outward from these reaction sites.[43] According to Taylor and Ervin the ignition and buildup sensitivities to shock can be separated.[43, 45] The formation of hot spots can be explained by several plausible mechanisms (void closure, microjetting in collapsing voids, plastic work at void peripheries, friction between particles, etc.).[43]

In the ignition and growth model a small fraction of the explosive is assumed to be ignited by the passage of the shock front, and the reaction rate is controlled by the pressure and surface area as in a deflagration process. The explosive material can be consumed very rapidly since the number of hot spots can be very large. Micronsized spherically burning regions grow and interact to consume the

intervening material within microseconds in most cases.[43] The Ignition and Growth reaction rate is given by the generalized equation:[43]

$$\frac{\partial F}{\partial t} = I(1-F)^x \eta^r + G(1-F)^x F^y p^z, \qquad (2.6.2)$$

where $\eta = V_0/V_1 - 1$ and F is the fraction of explosive that has reacted, t is time, V_0 is the initial specific volume of explosive, V_1 is the specific volume of shocked, unreacted explosive, p is pressure in megabars, and I, x, r, G, y, and z are constants. The most physically justifiable models have produced the best simulations of the experimental results.

The η^r term in Eq.(2.6.2) is used to investigate various hot-spot formation concepts, because η, is relative compression of the unreacted equation of state to any of the thermodynamic parameters that may be involved in the initiation process. To a good approximation, p is proportional to η^2 and the square of the particle velocity u_p^2 is proportional to η^3 over the range of compressions and pressures of interest in shock initiation.[43]

The second term in Eq. (2.6.2) describes the growth of the reaction. The constant G corresponds to a surface area to volume ratio and the p^z term represents a pressure dependent laminar burn rate.[43]

Nowadays the equation (2.6.2) is written in the form:

$$\frac{dF}{dt} = I(1-F)^b\left(\frac{\rho}{\rho_0} - 1 - a\right)^x + G_1(1-F)^c F^d p^y + G_2(1-F)^e F^g p^z, \qquad (2.6.3)$$

which represents the three stages of reaction generally observed during shock initiation and detonation of pressed solid explosive.[46, 47]

First stage of reaction, the first term in Equation (2.6.3) is the formation and ignition of hot spots caused by the various possible mechanisms discussed for impact ignition as the shock or compression wave interacts with the unreacted explosive molecules, $0 < F < F_{ig\,\max}$. For shock initiation modeling, the second term in Equation (2.6.3) then describes the relatively slow process of the inward and/or outward growth of the isolated hot spots in a deflagration-type process, $0 < F < F_{G_1\,\max}$. The third term in Equation (2.6.3) represents the rapid completion of reaction as the hot spots coalesce at high pressures and temperatures, resulting in transition from shock-induced reaction to detonation, $F_{G_2\,\min} < F < 1$.[47, 48]

For detonation modeling, the first term in Equation (2.6.3) again describes the reaction of quantity of explosive less than or equal to the void volume after the explosive is compressed to the unreacted von Neumann spike state. The second term in Equation (2.6.3) models the fast decomposition of solid into stable reaction product gases (CO_2, H_2O, N_2, CO, etc.). The third term in Equation (2.6.3) describes the relatively slow diffusion-limited formation of solid carbon (amorphous, diamond, or graphite) as chemical and thermodynamic equilibrium at the C-J state is approached.[47] These reaction zone stages have been observed experimentally using embedded gauges and laser interferometry to within several nanosecond resolution.[49, 50]

The Ignition and Growth reactive flow model has been applied to great deal of experimental shock initiation and detonation data using several one-, two-, and three-dimensional hydrodynamic codes. In shock initiation applications, it has successfully calculated many embedded gauge, run distance to detonation, short pulse duration, multiple shock, reflected shock, ramp wave compression, and divergent flow experiments on several high explosives at various initial

temperatures, densities, and degree of damage.[48] For detonation wave applications, the model has successfully calculated embedded gauge, laser interferometric metal acceleration, failure diameter, corner turning, converging, diverging, and overdriven experiments.[43, 50, 51, 52, 53, 54, 55, 56, 57]

2.7 DDT type ignition

In the initiation with the radiation of a diode laser or a CO_2 laser the surface of the explosive warms up inside a short time. If the consequence is the detonation, the initiation mechanism is from deflagration to detonation transition DDT.

According to many authors, the Lambert-Beer absorption $I/I_0 = e^{-\alpha x}$ might be one of the main interaction processes between the high explosive and the laser beam.[58, 59, 69, 80, 88] Here α is the absorption coefficient of the explosive material, x is the path length, I_0 is the incident light intensity and I is the transmitted light intensity. The absorption coefficient of the material α may have wavelength dependence.

According to the experiments, confinement has a strong role in the transition from warming up through deflagration to detonation. The initiation mechanism is at first stage thermal initiation. Thus the theoretical study of thermal initiation is valid in this case too.

The Frank-Kamenetskii equation for a single zero-order rate process is written in the form[60]:

$$-\lambda\left(\frac{\partial^2 T}{\partial x^2}+\frac{\partial^2 T}{\partial y^2}+\frac{\partial^2 T}{\partial z^2}\right)+\rho C(\partial T/\partial t)=\rho QZe^{-E_a/RT} \text{ or} \qquad (2.7.1)$$

$$-\lambda\nabla^2 T+\rho C(\partial T/\partial t)=\rho QZe^{-E_a/RT},$$

where T is temperature in K, λ is thermal conductivity, ρ is density, C is heat capacity, Q is heat of decomposition, Z is collision number, E_a is activation energy and R is the gas constant. Here it will be assumed that the above constants are independent of temperature. The Laplacian operator ∇^2 reduces in the cases of sphere, infinitely long cylinder, or infinite slab in one dimension to the form: $(\partial^2/\partial x^2) + (m\partial/x\partial x)$, where m = 0 for slab, 1 for cylinder and 2 for sphere. In some references the thermal conductivity λ is replaced in the Frank-Kamenetskii equation by the thermal diffusivity a.

When there are no chemical reactions, the reaction heating term $\rho QZe^{-E_a/RT}$ is zero and the equation (2.7.1) reduces to the heating equation:

$$\lambda\nabla^2 T = \rho C(\partial T/\partial t). \qquad (2.7.2)$$

In the one-dimensional case this equation has the form: $\partial^2 T/\partial x^2 = \rho C(\partial T/\lambda\partial t)$. For example in the case of infinite slap.

When the energetic material is illuminated by laser, in the case of laser ignition, the material absorbs the radiation E_{ls}, which is the total laser radiation E_{lstot} reduced by the reflected radiation E_{lsrefl}: $E_{ls} = E_{lstot} - E_{lsrefl}$. The laser power absorption term E_{ls} is expressed in two dimensional calculation by the equation[61]:

$$E_{ls}(r,z) = I(r)\cdot\alpha e^{-\alpha\cdot z}, \qquad (2.7.3)$$

where α is the absorption coefficient of the material, taking into account the Gaussian energy distribution of the laser beam $I(r) = I_0 e^{-r^2/w^2}$ (Eq. (3.2.1)), where I_0 is the ordinary intensity of the laser, r is the radial distance and w is the

beam radius[62]. The volumetric heating caused by the laser is thus equal to the material absorbed radiation E_{ls}, which can be described by the two dimensional equation:

$$E_{ls} \cong I_0(r,z,t)\frac{\alpha}{\lambda}e^{-r^2/w^2}e^{-\alpha\cdot z}, \tag{2.7.4}$$

where λ is the thermal conductivity. The laser intensity may have time dependence *t*. The equation (2.7.2) is writeable now in the form:

$$-\lambda\nabla^2 T + \rho C(\partial T/\partial t) = E_{ls}. \tag{2.7.5}$$

If the energetic material has a melting point T_m before the ignition, for example, in the case of RDX (Table 2.5.1), the heat of fusion ΔH_{fus} uses the energy of absorbed laser radiation, melting the material amount ∂m in the differential time unit ∂t. The heat of fusion is writeable in the form $\Delta H_{fus}(\partial m/\partial t)_{T_m}$. Equation (2.7.5) now has the form:

$$-\lambda\nabla^2 T + \rho C(\partial T/\partial t) + \Delta H_{fus}(\partial m/\partial t)_{T_m} = E_{ls}. \tag{2.7.6}$$

The term of net heat radiation loss rate takes the form $P(T) = e\sigma A(T^4 - T_s^4)$, which is provable from the Stefan-Boltzmann's law for the ideal blackbody radiator. Here e is the emissivity of the object ($e \le 1$ and $e = 1$ for the ideal radiator), σ is Stefan's constant ($\sigma = 5.6703\times10^{-8}\, W/m^2K^4$), A is the radiating area, T is the temperature of radiator and T_s is the temperature of surroundings. When the temperature is at the melting point T_m, $P(T) = e\sigma A(T_m^4 - T_s^4)$. Equation (2.7.6) reduces in the form:

$$-\lambda\nabla^2 T + \rho C(\partial T/\partial t) + \Delta H_{fus}\left(\partial m/\partial t\right)_{T_m} + P(T) = E_{ls} \qquad (2.7.7)$$

Energy comes into the system as the radiation of laser. Energy losses are the thermal conductivity (the term: $-\lambda\nabla^2 T$), the heat of fusion (the term: $\Delta H_{fus}(\partial m/\partial t)$) and the heat radiation (the term: $P(T)$).

If the system absorbs more energy of laser radiation than the energy losses are together, the temperature rises. The energetic material evaporates and there is another energy loss more, the heat of evaporation ΔH_v, which uses the energy of absorbing laser radiation evaporating the material amount ∂m in the differential time unit ∂t. The heat of evaporation has pressure dependence and it is writeable in the form $\Delta H_v\left(\partial m/\partial t\right)_p$. In some cases and with some explosives, the sublimation may be possible especially when the ambient pressure is low enough. The heat of sublimation ΔH_{sub} is thus an energy loss.[63]

The ignition energy (E_{ign}) is defined as the minimum amount of energy required to cause ignition, and corresponds to the ignition time.

The energy of the laser radiation excites the molecular vibrations in the energetic material. The energy in the phonon modes is transferred to the vibrations by multiphonon up-pumping processes.[13] As the vibration modes are excited, reactivity is enhanced and bond breaking due to thermal decomposition occurs in the molecule.[16]

The amount of energy, which is enough to excite the molecule just over the front of spontaneous reaction is the activation energy E_a. The breaking of the molecular bonds and the formulation of new molecules, the reaction products, is a highly exothermic process. Now the reaction heating term $\rho QZe^{-E_a/RT}$ is written on the right hand side of formula (2.7.5):

$$-\lambda\nabla^2 T + \rho C(\partial T/\partial t) + \Delta H_{fus}(\partial m/\partial t)_{T_m} + \Delta H_v(\partial m/\partial t)_p + P(T) = E_{ls} + \rho QZe^{-E_a/RT}$$
. (2.7.8)

The energy term E_{ls} is zero after the ignition pulse of laser. Energy losses are still the thermal conductivity, the heat of fusion ΔH_{fus}, the heat of evaporation ΔH_v and the heat radiation $P(T)$, but they are small compared with the reaction heating term.

$$-\lambda\nabla^2 T + \rho C(\partial T/\partial t) + \Delta H_{fus}(\partial m/\partial t)_{T_m} + \Delta H_v(\partial m/\partial t)_p + P(T) = \rho QZe^{-E_a/RT}.$$
(2.7.9)

The rate of the reactions is deflagration, but it accelerates to the steady state detonation in the environment of high confinement. This acceleration of reaction rate is called Deflagration to Detonation Transition. In the laser heating period of RDX the liquid phase and vapor phase occur and in the deflagration period the liquid phase occurs and thus the heat of fusion ΔH_{fus} and the heat of evaporation should be taken into account.[63] It seems probable that the heat of fusion ΔH_{fus} has no significant role in the case of steady state detonation. The radiation term *P(T)* is not insignificant when considering the energy balance. If it has been omitted, the result is just the equation (2.7.1) $-\lambda\nabla^2 T + \rho C(\partial T/\partial t) = \rho QZe^{-E_a/RT}$.

The Frank-Kamenetskii equation (2.7.1) has not been solved analytically. Numerical solutions can be obtained in some references.[17] The solution of the Frank-Kamenetskii equation under steady-state condition $(\partial T/\partial t) = 0$ leads to the equation:

$$-\lambda\left(\frac{\partial^2 T}{\partial x^2} + \frac{\partial^2 T}{\partial y^2} + \frac{\partial^2 T}{\partial z^2}\right) = \rho QZe^{-E_a/RT} \quad (2.7.10)$$

and to the expression for the critical temperature T_c in terms of related physical parameters.

$$T_c = \frac{E_a}{2.303R\ln(\rho a^2 QZE_a / \lambda RT_c^2 \delta)}, \qquad (2.7.11)$$

with the shape factor δ = 0.88 for slab, 2.00 for cylinder, and 3.32 for sphere. For a given size and shape of a given explosive material there is some maximum initial temperature which, if exceeded, will lead to a runaway reaction or explosion [14]. The iterative solution of the equation (2.7.11) gives values for T_c in certain conditions.

Experimental and calculated numerical values of critical temperatures T_c and some parameters in Frank-Kamenetskii equation of some high explosives are expressed in Table 2.7.1. Comp. B is a castable mixture of RDX and TNT in the proportion of 60:40. DATB is diaminotrinitrobenzene or 1,3-diamino-2,4,6-trinitrobenzene and TATB is triaminotrinirobenzene or 1,3,5-triamino-2,4,6-trinirobenzene. HNS is hexanitrostilbene. NQ is nitroguanidin. PETN is pentaerythitol tetranitrate and is known as Pentolite. RDX is trimethylentrinitramin or cyclo-1,3,5-trimethylene-2,4,6-trinitramine and is known as Cyclonite or Hexogen and also as T 4. TNT is 2,4,6-trinitrotoluene or trinitrotoluene and is known as Trotyl or also as Tolite.

HE	Sample Thickness d [mm]	T_c[°C] Exp.	T_c[°C] Calc.	a [cm]	ρ [g/cm^3]	Q [cal/g]	Z [s^{-1}]	E_a [cal/mol]	λ [cal/cmsK]
Comp B	0.80	216	215	0.040	1.58	758	4.62×10^{16}	43.1	0.00047
DATB	0.70	320-323	323	0.035	1.74	300	1.17×10^{15}	46.3	0.0006
HMX	0.80	258 253-255*)	253	0.033	1.81	500	5×10^{19}	52.7	0.0007
HNS	0.74	320-321	316	0.037	1.65	500	1.53×10^{9}	30.3	0.0005
NQ	0.78	200-204	204	0.039	1.63	500	2.84×10^{7}	20.9	0.0005
PETN	0.80	197 200-203*)	196	0.034	1.74	300	6.3×10^{19}	47.0	0.0006
RDX	0.80	214-217 215-217*)	217	0.035	1.72	500	2.02×10^{18}	47.1	0.00025
TATB	0.70	353 331-332*)	334	0.033	1.84	600	3.18×10^{19}	59.9	0.0010
TNT	0.80	286 287-289*)	291	0.038	1.57	300	2.51×10^{11}	34.4	0.0005

Table 2.7.1 Experimental and calculated numerical values of critical temperatures T_c and some parameters in Frank-Kamenetskii equation for high explosives.[14] *)[17]

The surface-to-volume rations of slab, cylinder, and sphere are 1/a, 2/a and 3/a, respectively, where a represents radius or half-thickness. According to the experiments and calculations a given value of the slab should have the lowest critical temperature. At relatively low temperatures explosion times relate to surface-to-volume ratios in the opposite manner. The sphere, having the smallest volume to be heated per unit surface, will explode fastest.[17]

2.8 Krause's exact differential equation of heat explosion

In the stationary temperature field, just before the runaway under steady-state condition, the Frank-Kamenetskii equation has the form (2.7.10), when the instationary term $(\partial T/\partial t) = 0$, and is so neglected. This implies a critical temperature distribution in the interior that is stable and stationary.[64]

The Frank-Kamenetskii equation (2.7.1) is based on the approximation $1/(1+x) \approx 1-x$. It results in the so called Frank-Kamenetskii transformation:

$$\exp\left(-\frac{E_a}{R}\frac{1}{T}\right) \approx \exp\left(-\frac{E_a}{R}\frac{1}{T_U}\right)\exp\left(-\frac{E_a}{R}\frac{\vartheta}{T_U^2}\right), \tag{2.8.1}$$

where T_U is the ambient temperature and $\vartheta = T - T_U$ is the temperature difference. The term $\Theta = (E_a / R)/(\vartheta/T_U^2)$ is a dimensionless variable.

According to Krause, the exact equation of heat explosion will be derived without any approximation. The stationary equation (2.7.10) is written with the Laplace's operator in the form of Fourier's heat equation:

$$\nabla^2 T = -Q_0 \frac{1}{a} e^{-E_a/RT}, \tag{2.8.2}$$

where $Q_0 = \rho QZ/C$ and thermal conductivity λ is replaced by thermal diffusivity a. The temperature difference $\vartheta = T - T_U$ and the dimensionless coordinate $\xi = x/L$ permit the derivation from equation (2.8.2) of the one dimensional relationship:[64]

$$\frac{\partial^2 \vartheta}{\partial \xi^2} = -Q_0 \frac{1}{a} e^{-E_a/RT} . \tag{2.8.3}$$

The definition of a dimensionless temperature $\Theta = 1 + (\vartheta/T) = T/T_U$ transforms the equation (2.8.2) into the expression:

$$\frac{\partial^2 \Theta}{\partial \xi^2} = -Q_0 \frac{1}{a} L^2 \frac{1}{T_U} \exp\left(- \frac{E_a}{RT_U} \frac{1}{\Theta} \right), \tag{2.8.4}$$

which is the exact, stationary differential equation of heat explosion.[64] Two new dimensionless parameters are defined according to:

$$\delta_1 = Q_0 \frac{1}{a} L^2 \frac{1}{T_U} \tag{2.8.5}$$

and

$$\delta_2 = \frac{E_a}{R} \frac{1}{T_U} . \tag{2.8.6}$$

The heat explosion equation (2.8.4) appears now in the final dimensionless form:

$$\frac{\partial^2 \Theta}{\partial \xi^2} = -\delta_1 \exp\left(- \frac{\delta_2}{\Theta} \right), \tag{2.8.7}$$

which posses two parameters δ_1 and δ_2 whereas the equation of Frank-Kamenetskii contains one parameter only.[64] The ambient temperature T_U has been eliminated from equations (2.8.5) and (2.8.6) by forming the quotient:

$$\frac{\delta_1}{\delta_2} = \delta_{12} = \frac{Q_0}{\lambda} \frac{R}{E_a} L^2 . \tag{2.8.8}$$

The fundamental relation (2.8.7) contains all the necessary information about the substance, such as thermal diffusivity a (or thermal conductivity λ), Arrhenius prefactor Q_0, apparent activation energy E_a/R and characteristic length L. Table 2.8.1 compares the parameters in Frank-Kamenetskii equation and Krause's equation (2.8.7).

Frank-Kamenetskii	**Krause**
$\frac{\partial^2\Theta}{\partial\xi^2} = -\delta_{FK}\exp(\Theta)$	$\frac{\partial^2\Theta}{\partial\xi^2} = -\delta_1\exp\left(-\frac{\delta_2}{\Theta}\right)$
$\Theta = \frac{E_a}{RT_U}\frac{T-T_U}{T_U}$	$\Theta = \frac{T}{T_U}$
$\delta_{FK} = \frac{Q}{a}\frac{E_a}{R}\frac{1}{T_U^2}\exp\left(-\frac{E_a}{RT_U}\right)\cdot L^2$	$\delta_1 = Q_0\frac{1}{a}L^2\frac{1}{T_U}$
	$\delta_2 = \frac{E_a}{R}\frac{1}{T_U}$
	$\delta_{12} = \frac{Q_0}{\lambda}\frac{R}{E_a}L^2$

Table 2.8.1 The comparison between the parameters of Frank-Kamenetskii's equation and Krause's equation.[65]

It is not possible to solve equation (2.8.7) using analytical methods.[64] A numerical solution with the aid of finite difference formulae is performed.[65]

2.9 SDT type ignition

According to the experimental studies of shock initiation of homogenous explosives the detonation of the heated, compressed explosive begins at the interface, where the explosive has been hot the longest, after an induction time, which is a decreasing function of the shock strength.[15] The initiation mechanism is known as from shock to detonation transition (SDT). The detonation proceeds through the compressed explosive at a velocity greater than the steady state velocity in uncompressed explosive, overtaking the initial shock and overdriving the detonation in the unshocked explosive.[17]

The shock-initiated molecular reactions require transfer of substantial amount of mechanical energy from the shock front to the internal vibrational states of the molecules. This process is known as the multiphonon up-pumping.[13]

An explosive is shocked with a square-wave pulse shock wave, which has an amplitude *P*, the shock pressure, and a duration *t*, the shock width in the time scale. The particle velocity behind the shock front is *u*. The rate at which work is done per unit area on the energetic material being compressed by the shock is: rate of work/unit area = *Pu*. The amount of energy per unit area or the energy fluence, *E*, deposited in the energetic material is:

$$E = Put\,. \qquad (2.9.1)$$

Taking into account the conservation equations of mass and momentum for shock derives:

$$P = \rho_o u U\,, \qquad (2.9.2)$$

where ρ_o is the density of unshocked material and U is the shock velocity. For the particle velocity *u* is writeable as: $u = P/(\rho_o U)$. Equation (2.9.1) gives now:

$$E = P^2 t / (\rho_o U). \qquad (2.9.3)$$

The quantity $\rho_o U$ is called the shock impedance of a material. It increases very slowly with increasing pressure, but over the pressure ranges of general interest in shock initiation it can be considered to be nearly constant. Because of this, $P^2 t$ is frequently used instead as the critical value for initiation.[14]

The square-wave shock pulses are simulated experimentally by the impact of flyer plates. The pulse duration is varied by changing the thickness of the flyer plates, and the shock pressure is varied by changing the impact velocity of the flyer plates. According to the experiments each explosive is found to have a unique range of energy fluence, above which prompt detonation is always obtained, and below which it is not.[14] The average of this range is called the critical energy fluence, E_c.

Table 2.9.2 lists critical energy fluence for shock initiation for number of various energetic materials. HNS-I is a kind of hexanitrostilbene (HNS), which has a less pure raw product with lower bulk density compared with HNS-II.[66] NM is nitromethane. PBX-9404 is a plastic-bonded explosive, which contains 94% of HMX. Tetryl is tetranitromethylanilin or trinitro-2,4,6-phenylmethylnitramine and is also known as Pyronite.

Explosive	Density ρ [g/cm^3]	E_c [cal/cm^2]	E_c [J/cm^2]
Comp. B	1.73	44	184
DATB	1.676	39	163
HNS-I	1.555	<34	<142
Lead azide	4.93	0.03	0.13
NM	1.13	405[a]	1694[a]
PBX-9404	1.84	15	63
PETN	1.0	2.7	11
PETN	1.6	4	17
RDX	1.55	16[b]	67[b]
TATB	1.762	72-88	301-368
Tetryl	1.655	10	42
TNT, cast	1.6	100[a]	419[a]
TNT, pressed	1.645	34	142

Table 2.9.2 Critical energies for shock initiation of some energetic materials.[67] ([a]Values are estimated from data other than critical energy determinations and should be considered tentative. [b]Constant energy threshold not confirmed.[67])

3. Diode laser ignition of energetic materials

3.1 Introduction

The use of laser as an ignition source has been extensively applied to studies of the ignitability of explosives and pyrotechnical materials. Laser was first introduced as an ignition source for energetic materials by Brish et al[68, 69] and Menichelli and Yang[70, 71] in the sixties and early seventies. They carried out the studies using a Q-Switched Ruby laser and a Nd:YAG-laser, which has also been the laser pulse source in the subsequently published studies[72, 73, 74, 75]. The ignition mechanism was from shock to detonation transition (STD). Laser ignition studies on both deflagration and detonation with a CO_2 laser have been carried out by many authors[76, 77, 78, 79, 80, 81, 82]. The ignition mechanism with explosives was from deflagration to detonation transition (DDT). One significant result of the experiments is the strong dependence between the energy necessary for ignition and the surrounding gas pressure. A conclusion has been drawn that the ignition process is not only a solid phase reaction but is a complex process where gas, liquid and/or solid phase reactions are involved. The diode laser has been used as an ignition device for pyrotechnic mixtures or propellants and for explosives by an increasing number of authors[83, 84, 85, 86, 87]. Theoretical descriptions and numeric modeling of laser ignition have been published in many papers[84, 88, 89, 90, 91, 92, 93].

3.2 Methods and experimental setup

The diode laser ignition studies of explosives by means of optical fiber were carried out as a function of ambient overpressure. Apparatus was developed specially for diode laser ignition research, consisting of a laser ignition test device and a pressure chamber (Fig. 3.2.1). The Up-and-down method[94] (Appendix 1)

was applied using the ambient pressure of 10, 20, 30, 40 and 50 bar, when the parameter was the diode laser current. The pulse duration of 100 ms was used.

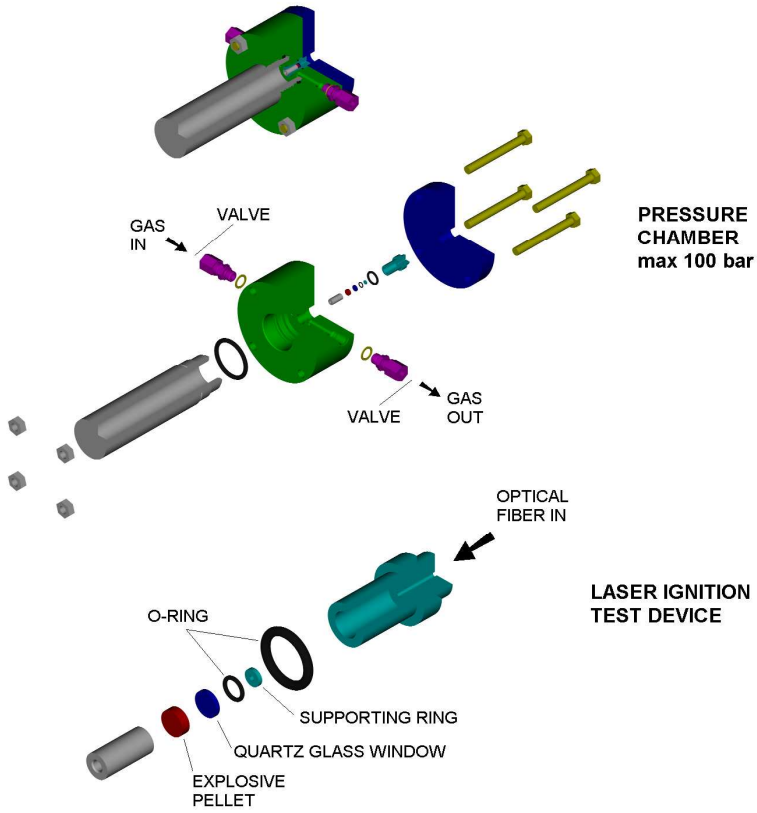

Fig. 3.2.1 The complete pressure chamber (top) and the laser ignition test device disassembled (middle). The test device components depicted on a larger scale (bottom).

In the Fig. 3.2.2 depicts the experimental setup of laser ignition studies schematically. The core diameter of the optical fiber was 0.8 mm. Between the explosive pellet and the end of the optical fiber there was a 1 mm thick quartz class window. The monitoring of the initiation was carried out using optical fiber and a photo detector (Oriel 70124) with a transient recorder (IMC Cronos with the FAMOS computer program). The diode laser used

was 2.6 W, 808 nm, (Coherent-Tutcore, F-8 10-10-260-20SMM) with a microcomputer controlled power supply and temperature control customized for diode laser ignition measurements (Coherent-Tutcore). The laser energy was measured with LaserMate-P Energy Meter combined with a crystalline pyroelectric detector (Coherent). The profile of the laser beam on the surface of the energetic material was measured with a CCD camera based laser beam imager (WinCamD). The mean specific gravity of the pressed RDX pellets was 1.65.

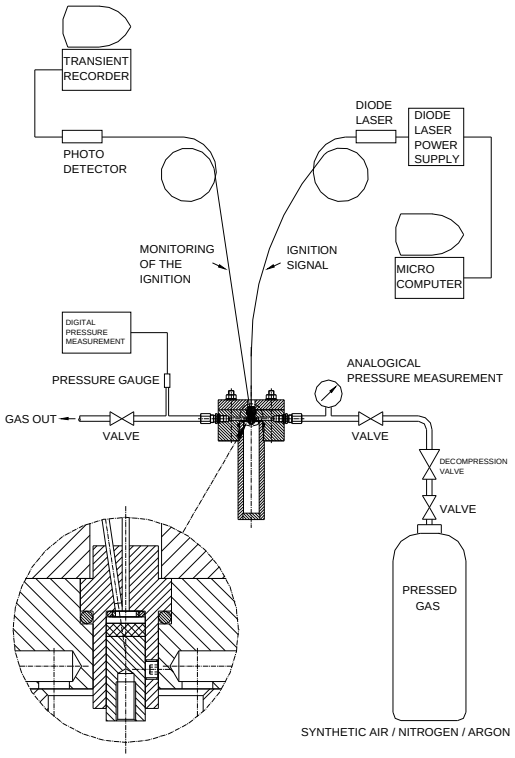

Fig. 3.2.2 The schematic picture of the experimental setup. The monitoring of the initiation was carried out using optical fiber and a photo detector.

A typical profile of the laser beam is depicted in Fig. 3.2.3. The profile was measured at a distance of 1 mm from the fiber using the CCD camera based laser beam imager. The cross section of the profile is the Gaussian shape having a sharp intensity maximum on the plane of illuminated explosive surface. The

spatial intensity distribution $I(r)$ as a function of radial distance r can be written as the equation:

$$I(r) = I_0 e^{-r^2/w^2}, \qquad (3.2.1)$$

where I_0 is the center intensity and w is the beam radius[62]. The mean root diameter of the typical profile is 0.9 mm and the diameter of the half maximum is 0.3 mm, respectively. The area of the beam on the explosive surface is approximately 0.65 mm^2.

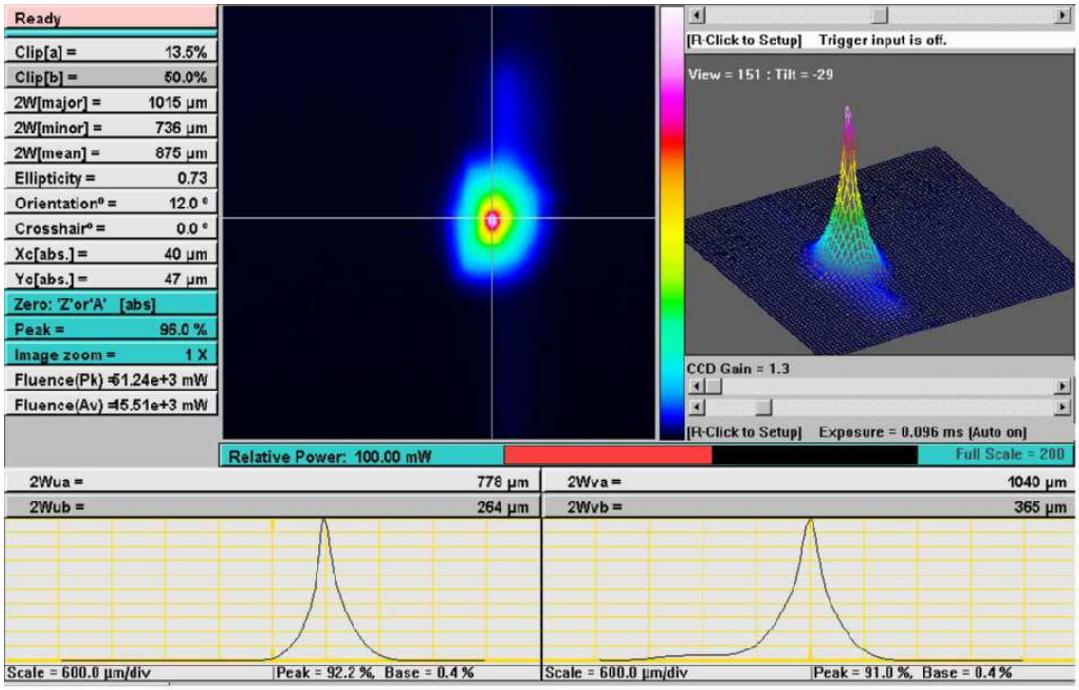

Fig. 3.2.3 A typical profile of the laser beam on the virtual surface of RDX pellet measured using the CCD camera based laser beam imager. The distance between the end of the fiber and the CCD detector was 1 mm.

3.3 Diode laser ignition of explosives

The diode laser ignition properties of different energetic materials are important when the ignition mechanisms are investigated or the best or most suitable material for a current laser ignition application are chosen. One of the most important variables is the ignition energy. Thus it is reasonable to study the minimum ignition energy of many energetic materials and choose the best material among them. Other criteria may be, for example, the detonation properties of the current material as a booster or an igniter and the ageing properties of the current material.

Figure 3.3.1 compares the diode laser ignition energies of 12 different explosives. The numerical values of the ignition energies and comparable ignition currents are presented in Table 3.3.1. The pressure in the confinement was 50 bar synthetic air. The length of the laser pulse was 100 ms. The ignition mechanism was from deflagration to detonation transition. FPX7[a] is a RDX based plastic bonded explosive. P1[a] is a plastic bonded pentolite (PETN) booster explosive.

[a] TM of OY FORCIT AB

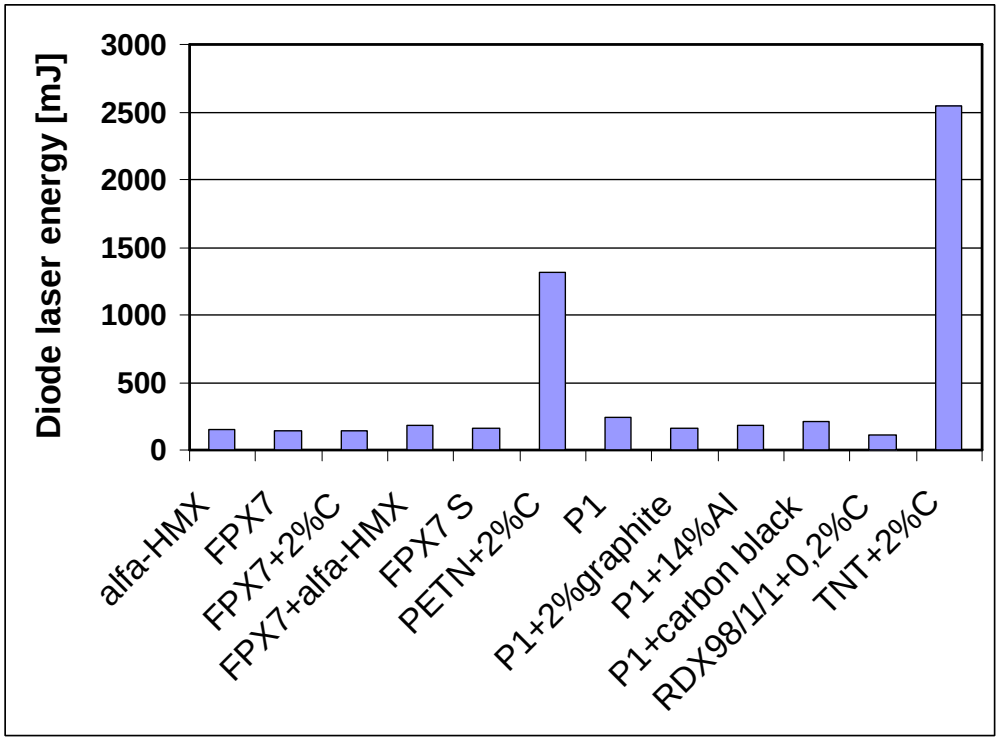

Fig. 3.3.1 Diode laser ignition energy of some explosives, when the synthetic air pressure is 50 bar.

Explosive	I[A]	E_{laser}[mJ]	$E_{ignition}$[mJ]
alfa-HMX	1.9	155.8	70
FPX7	1.7	139.4	54
FPX7+2%C	1.7	139.4	54
FPX7+alfa-HMX	2.2	180.4	77
FPX7 S	2	164	56
PETN+2%C	16	1312	300
P1	3	246	110
P1+2%graphite	2	164	56
P1+14%Al	2.2	180.4	83
P1+carbon black	2.6	213.2	94
RDX98/1/1+0,2%C	1.4	114.8	35
TNT+2%C	31	2542	770

Table 3.3.1 Numerical values of diode laser ignition current and comparable ignition energy for some high explosives, when the synthetic air pressure is 50 bar.

Table 3.3.1 depicts the absorption of the laser radiation on the explosive surface and in the explosive, when the wavelength of the diode laser is 808 nm. The reflecting angle is 45^{o}.

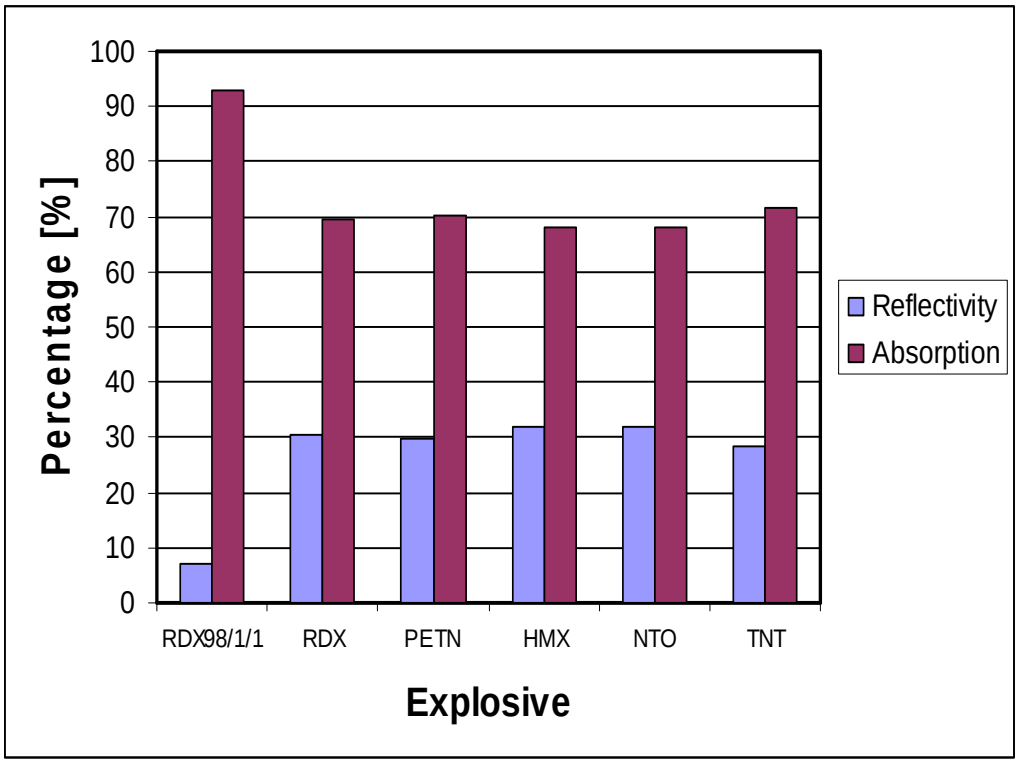

Fig. 3.3.2 Reflectivity to the 45^{o} angle and absorption of diode laser radiation on the surface of explosive as percentage, when the wavelength is 808 nm.

Explosive	Reflectivity	Absorption
RDX98/1/1	7.3	92.7
RDX (pure)	30.6	69.4
PETN	29.9	70.1
HMX	31.8	68.2
NTO	32.0	68.0
TNT	28.4	71.6

Table 3.3.2 Numerical values of reflectivity to the 45^{o} angle and absorption of diode laser radiation on the surface of explosive as percentage, when the wavelength is 808 nm.

The ignition current carbon black content dependence of RDX was measured from 1% to 3%. According to the experiments the mechanical properties of the RDX pellet are fragile at higher carbon black contents. Results are depicted in Fig. 3.3.3.

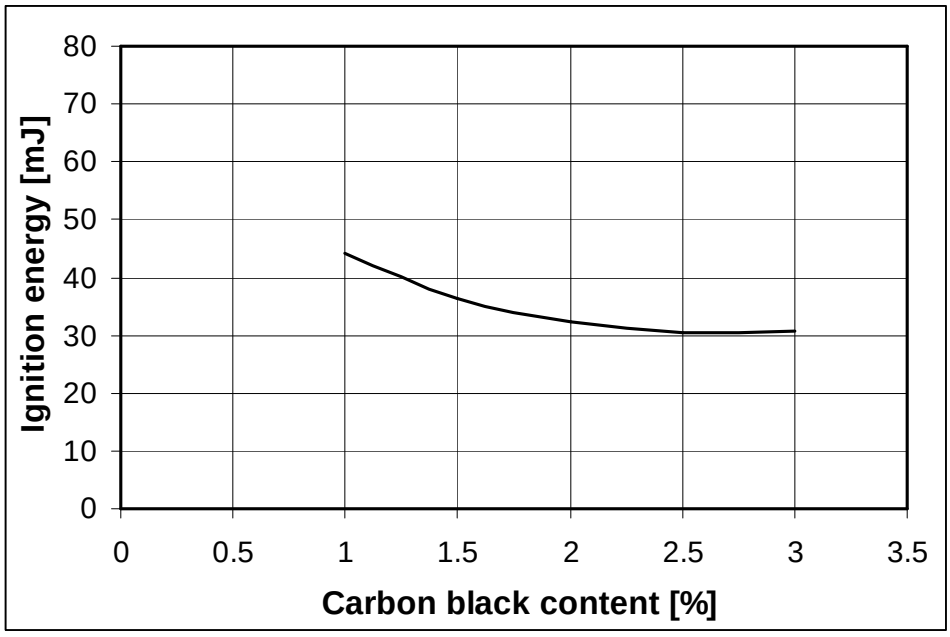

Fig. 3.3.3 Ignition energy of RDX as a function of carbon black content, when the pressure is 50 bar. The wax content was 1%.

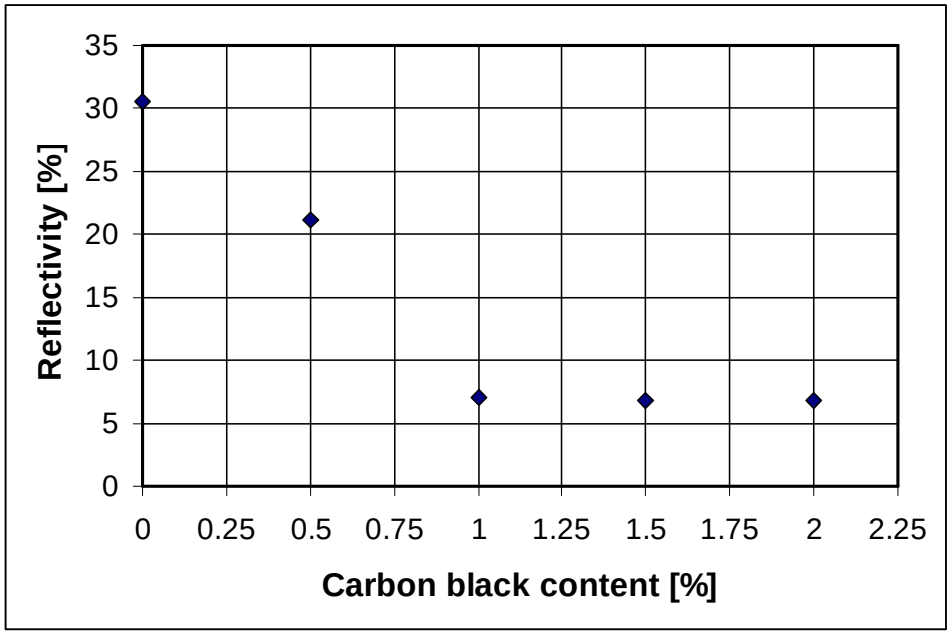

Fig. 3.3.4 Reflectivity of RDX as a function of carbon black content. The wax content was 1%.

Carbon black content [%]	Reflectivity [%]	Variation [+/-%]
0	30.6	1.8
0.5	21.1	1.4
1	7.1	0.5
1.5	6.8	0.4
2	6.8	0.4

Table 3.3.3 Reflectivity of RDX as a function of carbon black content. The wax content was 1%.

According to the reflectivity measurements, RDX98/1/1 absorbs about 93% of the diode laser radiation at the wavelength of 808 nm. According to the results depicted in Fig. 3.3.4 and Table 3.3.3, the 1% carbon black content increases the

absorption of the 808 nm diode laser radiation on the surface of RDX98/1/1 by about 23% when compared with pure RDX.

The spectroscopic methods give 17% reflectance for RDX98/1/1 and 96% reflectance for pure RDX, when the wavelength is 808 nm (12376 cm^{-1}). Fig. 3.3.5 depicts the emission spectra of pure RDX and RDX98/1/1 in the visible wavelength range and in the near infrared range. In the near infrared spectra of pure RDX the typical characteristics of vibration and rotation lines of RDX molecule are identifiable. The Spectra were measured using a dispersive Perkin Elmer Lamda 900 UV VIS NIR spectrophotometer.

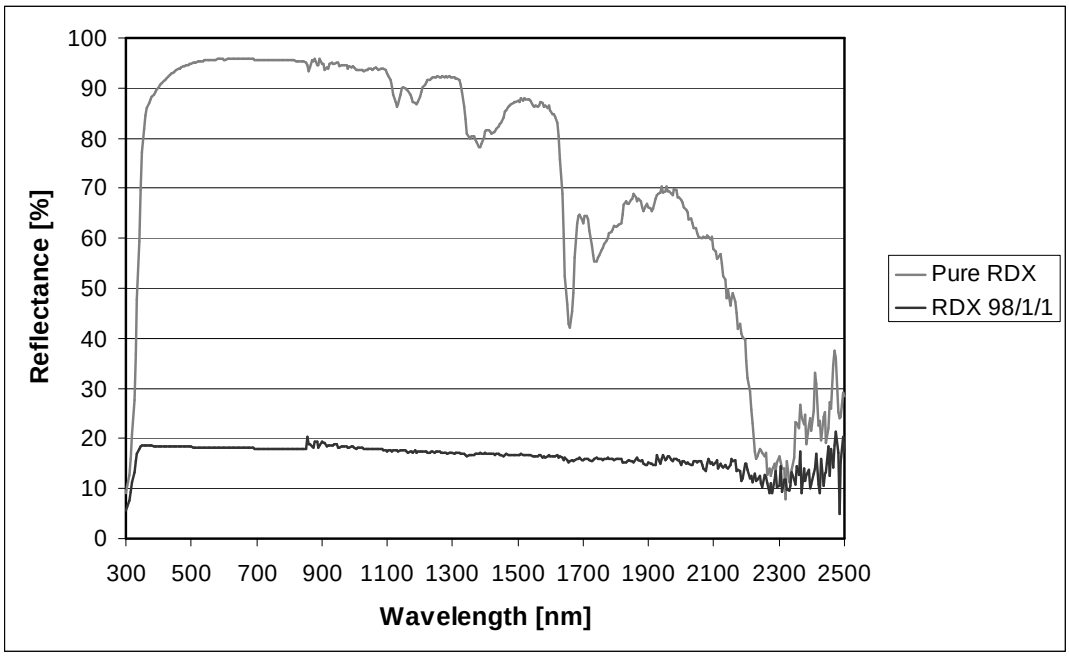

Fig. 3.3.5 Emission spectra of pure RDX and RDX98/1/1 from the wavelength of 300 nm to the wavelength of 2500 nm.

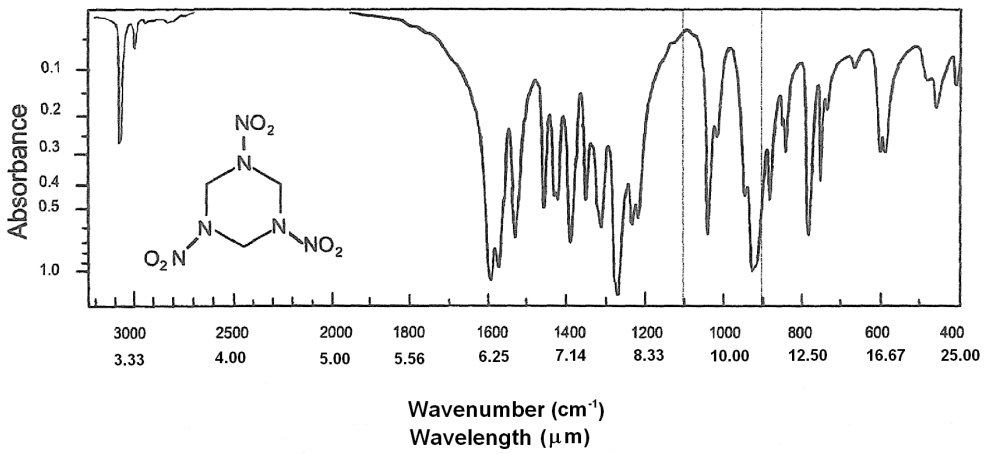

Fig. 3.3.6 IR absorbance spectrum of pure RDX from the wavelength of 3 μm to the wavelength of 25 μm (1 μm = 1000 nm). Hatched lines enclose the wavelength domain accessible by the CO_2 laser[82].

3.4 Laser ignition of RDX

The diode laser current at 5%, 50% and 95% ignition probability for RDX/1/1.2 (1% wax and 1.2% carbon black) as a function of pressure is depicted in Fig 3.4.1. The diode laser current at 95% ignition probability is 5 A, when the pressure is 10 bar, and decreases to 1.4 A, when the pressure is 50 bar. The ignition energy is 180 mJ and 32.6 mJ (Fig. 3.4.4), corresponding to the mean energy density of 29.9 J/cm^2 and 5.4 J/cm^2 (Fig. 3.4.5), respectively, which are in good agreement with the corresponding energy density values published in the reference[72].

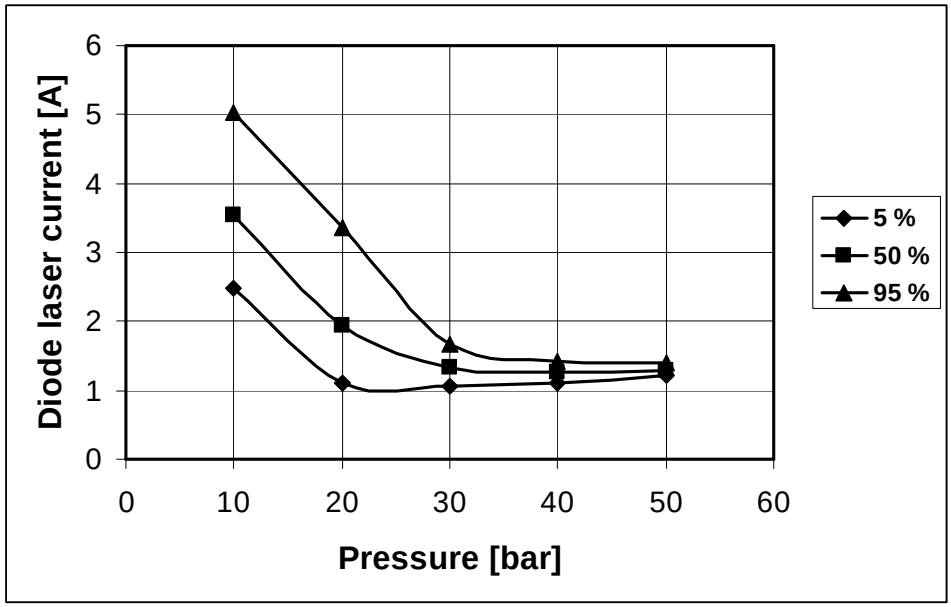

Fig. 3.4.1 Diode laser ignition current for RDX/1/1.2 as a function of pressure at 5%, 50% and 95% ignition probability.

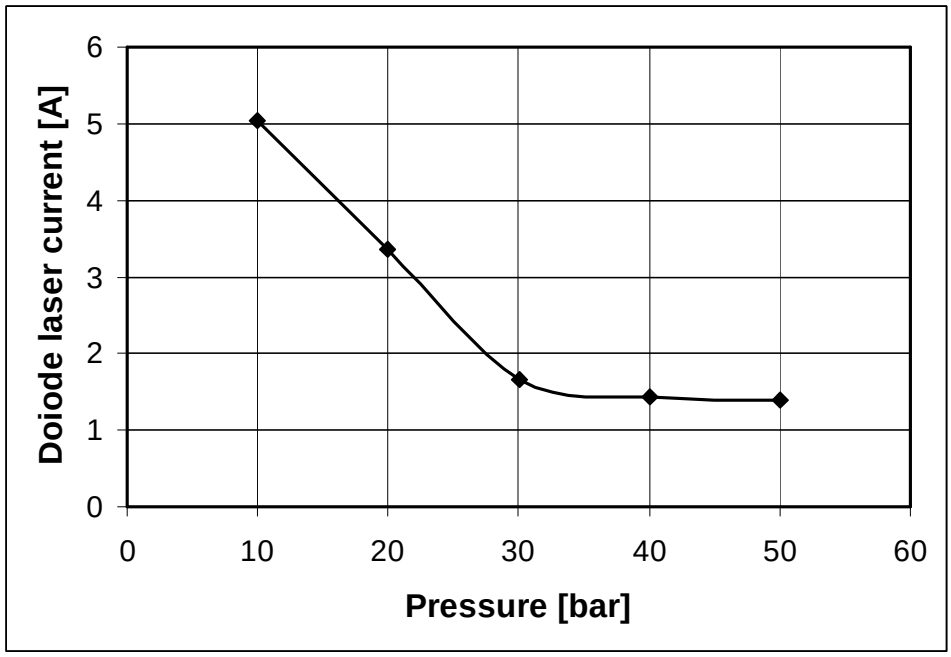

Fig. 3.4.2 Diode laser ignition current for RDX/1/1.2 as a function of pressure.

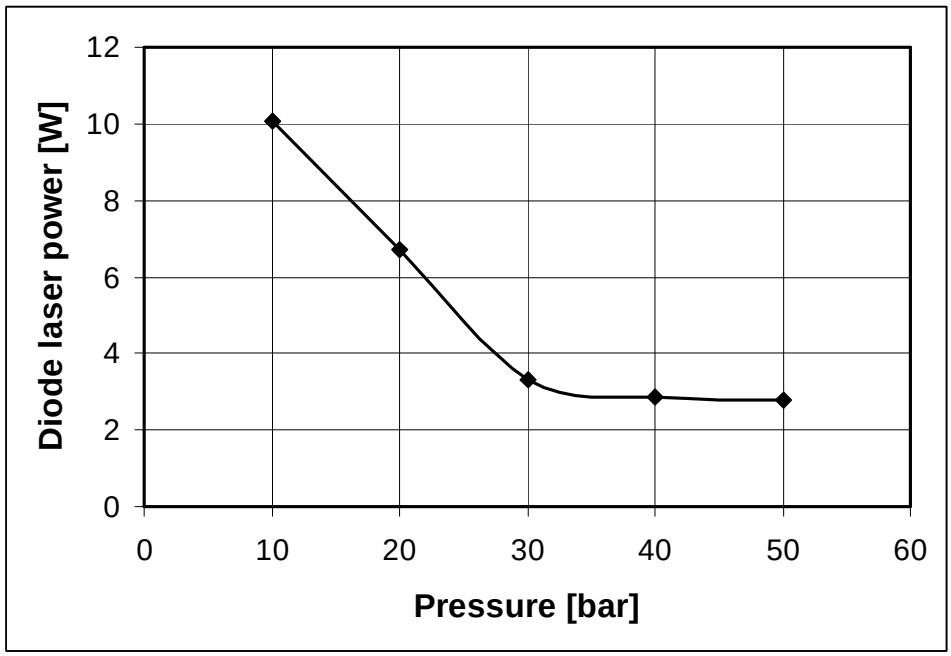

Fig. 3.4.3 Diode laser ignition power for RDX/1/1.2 as a function of pressure.

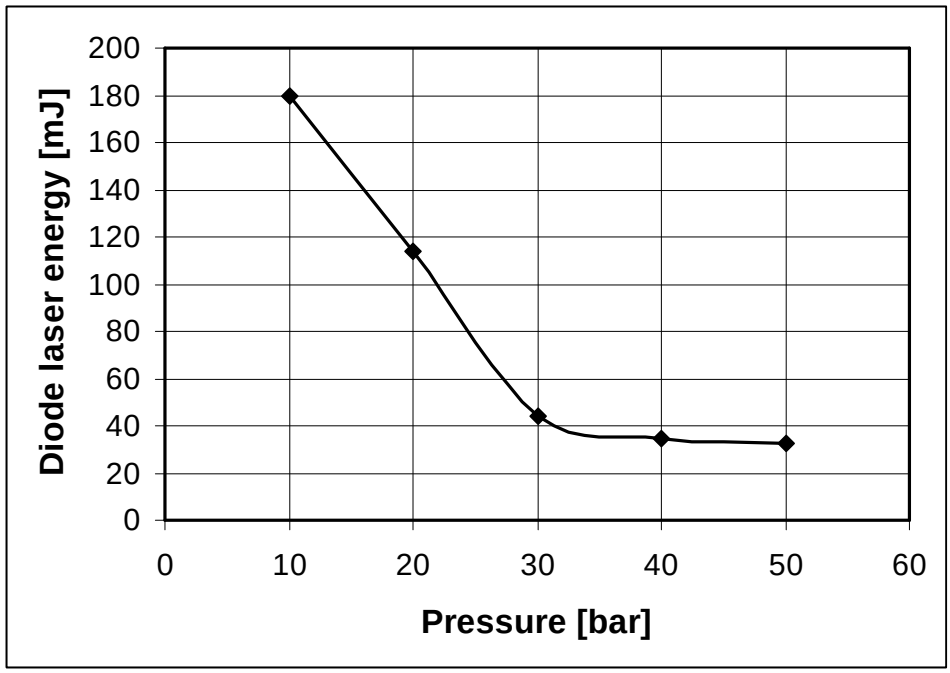

Fig. 3.4.4 Diode laser ignition energy for RDX/1/1.2 as a function of pressure.

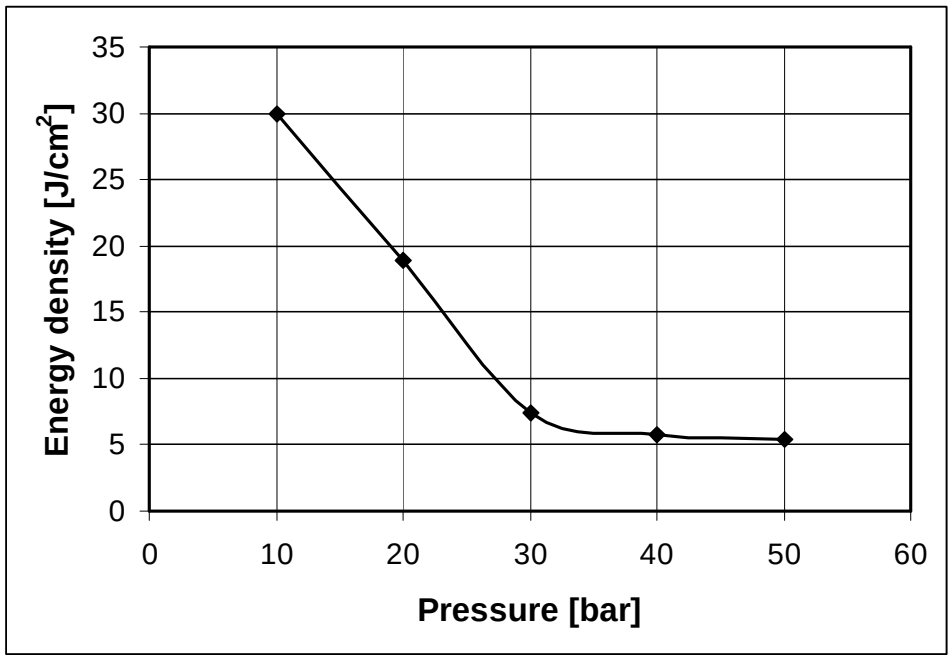

Fig. 3.4.5 Mean ignition energy density of laser light on the surface of RDX pellet as a function of pressure.

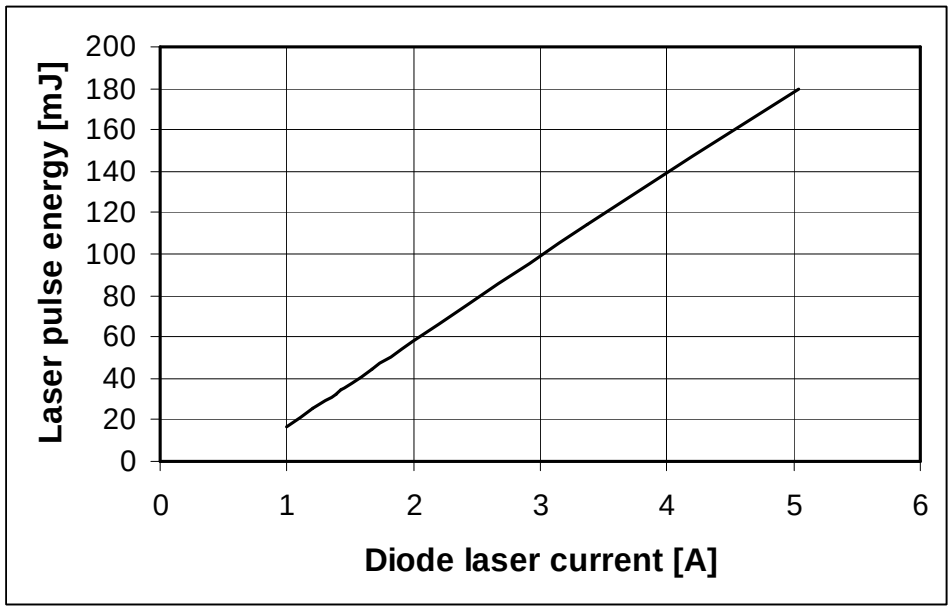

Fig. 3.4.6 Energy of laser pulse as a function of diode laser current.

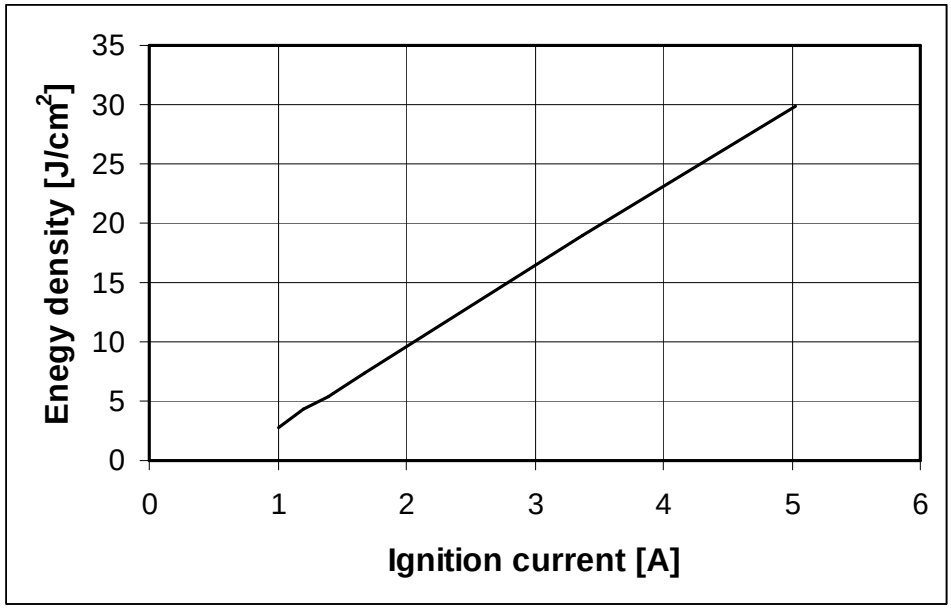

Fig. 3.4.7 Mean energy density on the surface of RDX pellet as a function of diode laser current.

Pressure [bar]	Laser Power [W]	Ignition energy density [J/cm2]
10	10.1	29.9
20	6.7	19.0
30	3.3	7.4
40	2.9	5.7
50	2.8	5.4

Table 3.4.1 Equivalence between the pressure, diode laser power and mean ignition energy density on the surface of RDX pellet.

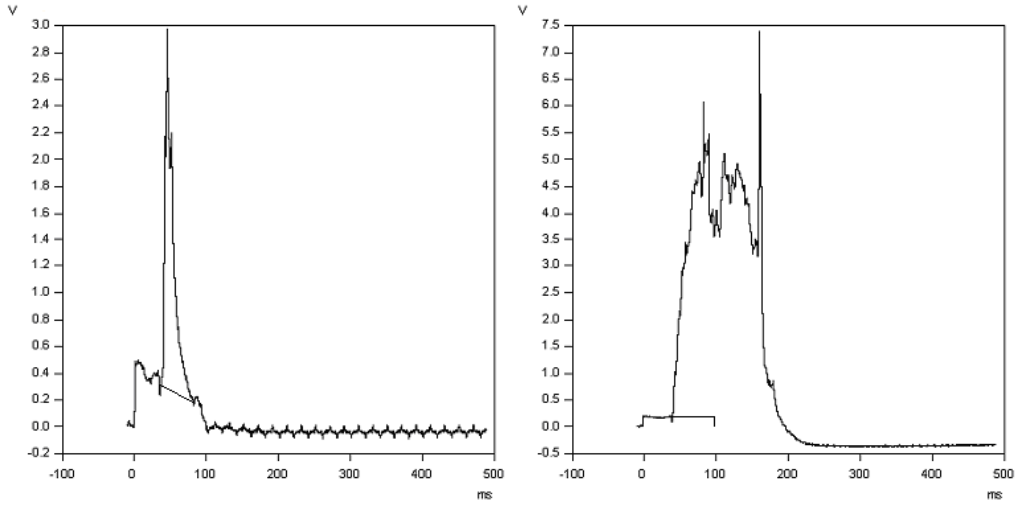

A) B)

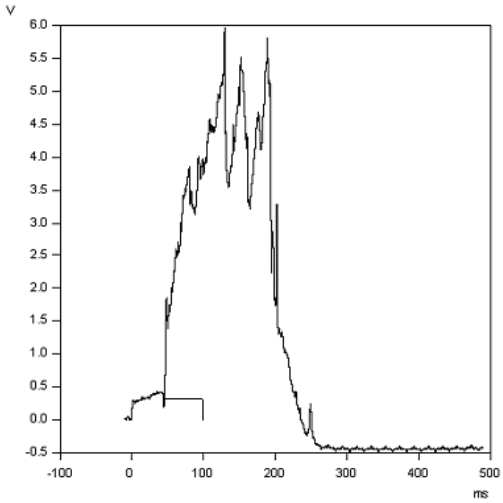

C)

Fig. 3.4.8 Typical cases in the laser ignition experiments with RDX. The duration of the laser pulse was 100 ms.

Fig. 3.4.8 depicts the typical cases in the laser ignition experiments with RDX. In picture A) the initiation begins as a deflagration 36 ms after the beginning of the laser pulse and the state changes immediately into a detonation. In picture B) the initiation begins as a deflagration 39 ms after the beginning of the laser pulse. The

RDX-pellet deflagrates and after 110 ms the reaction changes into a detonation. In picture C) the initiation begins 46 ms after the beginning of the laser pulse. The duration of the deflagration is 210 ms and probably no transition to detonation happened.

The mean time from the start of the ignition pulse to the initiation was 43 ms ± 7 ms, when energetic material was RDX98/1/1 and the pressure in the sample chamber was 50 bar.

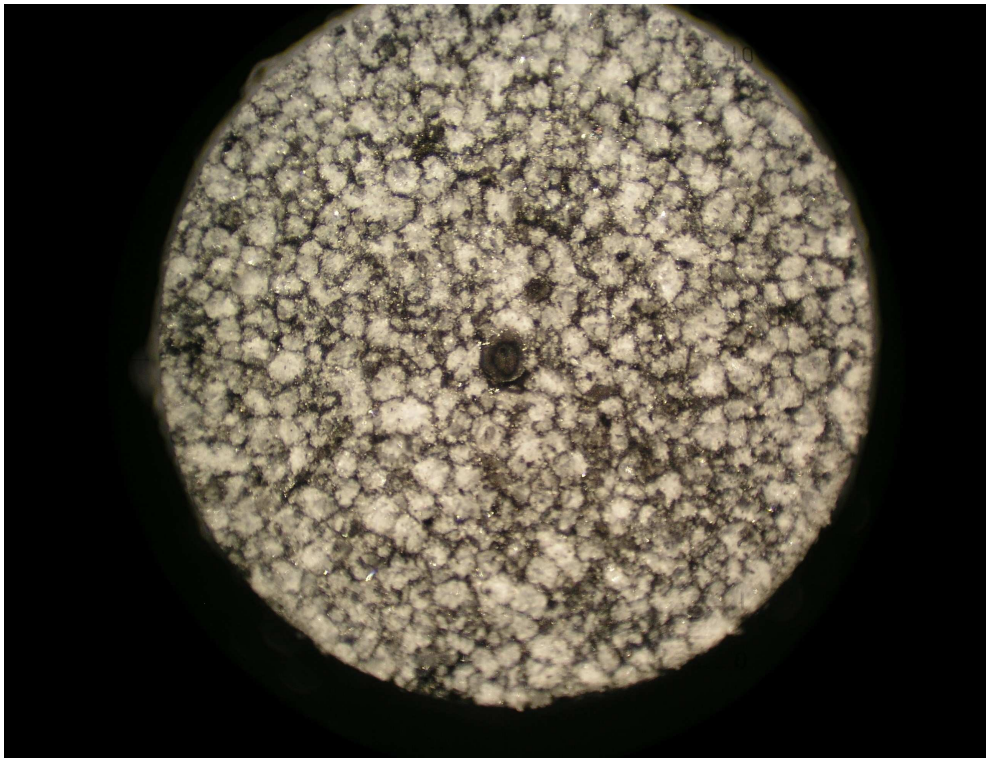

Fig. 3.4.9 The illuminated point of the laser beam on the surface of the RDX pellet just below the minimum ignition energy in the case of high confinement, when the pressure is 50 bar and the energy of the laser beam is 17 mJ. The diameter of the pellet is 6 mm. The diameter of the molten point on the surface of the pellet is about 0.3 mm.

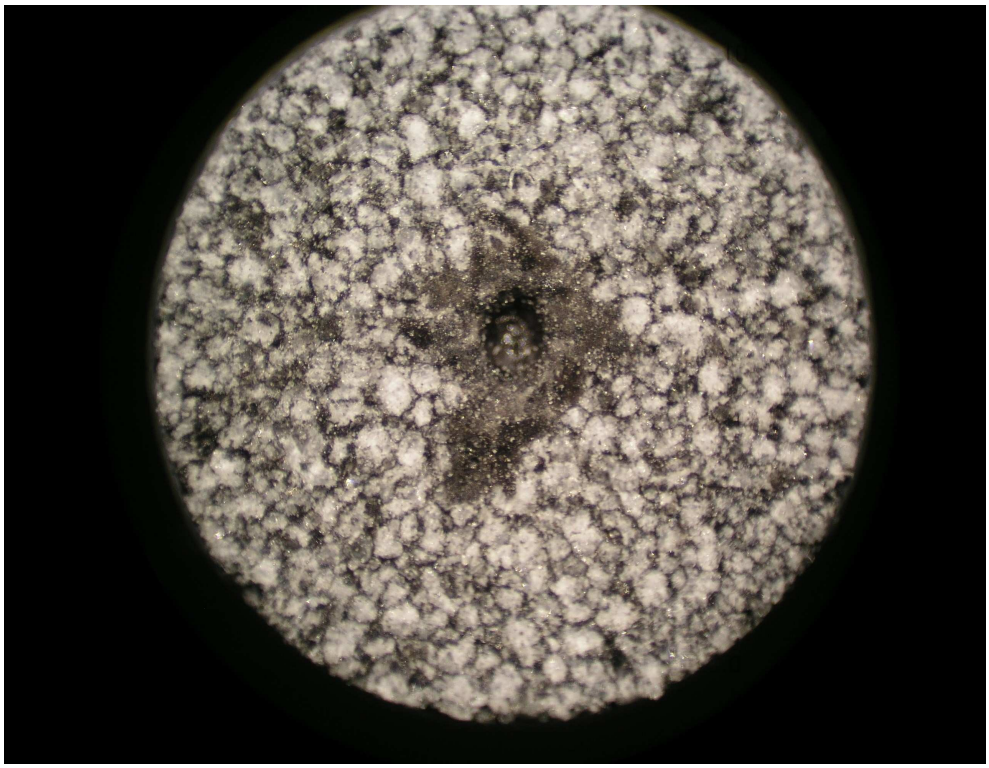

Fig. 3.4.10 The illuminated point of the laser beam on the surface of the RDX pellet in the case of low confinement, when the pressure is 1 bar and the energy of the laser beam is 65 mJ.

3.5 Confinement in the DDT type laser ignition and discussion

Confinement is understood as a local physical state of things on the surface of energetic material or in the bulk of energetic material, where the pressure will go quickly high enough to increase the detonation velocity or bring it closer to the ideal performance.[14] It can cause the start of a spontaneous detonation reaction from the initial state, such as combustion or deflagration, as is the situation in the DDT type laser ignition.

Fig 3.5.1 depicts the laser ignition results for RDX98/1/1 (+1% extra carbon black) as a variable diode laser current of the Up-and-Down method, when the ambient pressure of the RDX pellet was 50 bar with synthetic air, nitrogen and argon. The laser pulse width was 100 ms. The numerical values are presented in the Table 2.5.1. The ignition currents are in practice the same for synthetic air and argon, but nitrogen gives slightly higher ignition current.

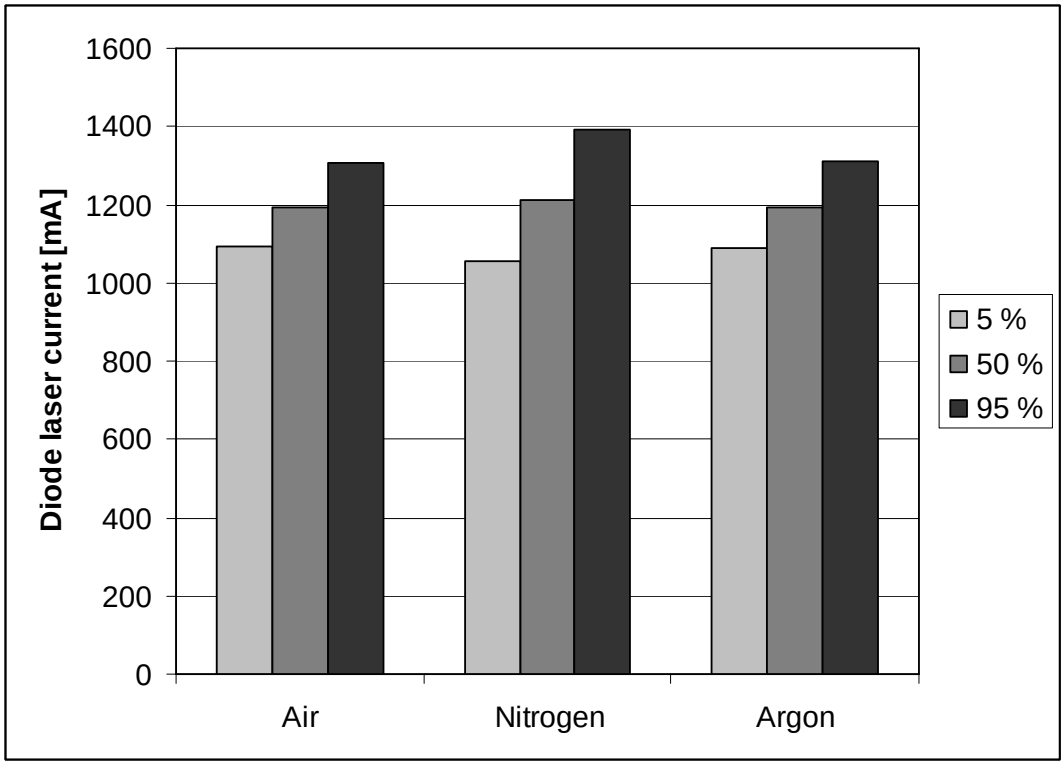

Fig. 3.5.1 Percentage ignition probability of RDX as a function of diode laser current, when the pressure of synthetic air, nitrogen and argon is 50 bar.

Ignition probability	Air	Nitrogen	Argon
5%	1091.8	1054.9	1088.5
50%	1193.4	1212.1	1193.7
95%	1304.5	1392.7	1309.2

Table 3.5.1 Numerical values of diode laser current for the percentage ignition probability - 5%, 50% and 95% - of RDX, when the pressure of synthetic air, nitrogen and argon is 50 bar.

These results suggest that the oxygen (in synthetic air) may have no reactions or the reactions are not remarkable in the laser illuminated point of RDX pellet in this experimental setup. Östmark et al.[79] achieved analogous results - air versus nitrogen - for PETN, when the pressure was lower than 45 bar and for RDX, when the pressure has been lower than 20 bar. For the higher pressures the results are in reverse order. In the experimental setup of Östmark, the laser illuminated point on the surface of explosive is open to the half of full solid angle. In this experimental setup, the quartz glass confines the laser illuminated point on the surface of explosive pellet.

Figure 3.5.2 depicts typical condensation of RDX on the surface of quartz glass a) (I) and b), when the laser energy is just below the minimum ignition energy in the case of high confinement. The pressure of argon was 50 bar.

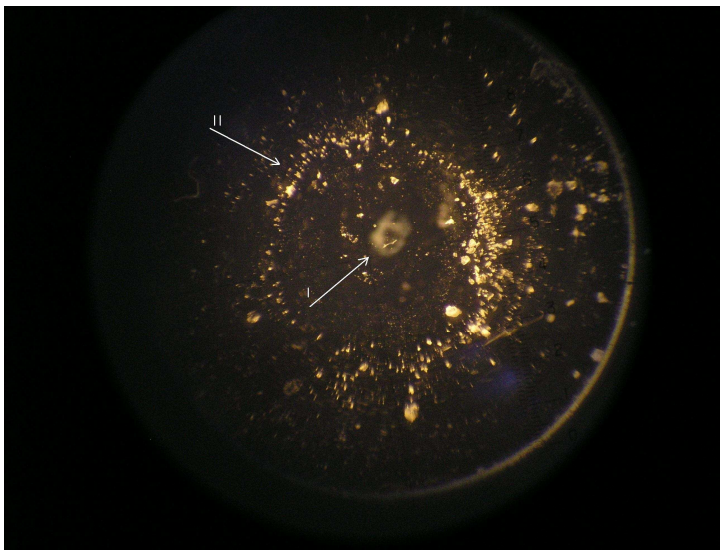

a)

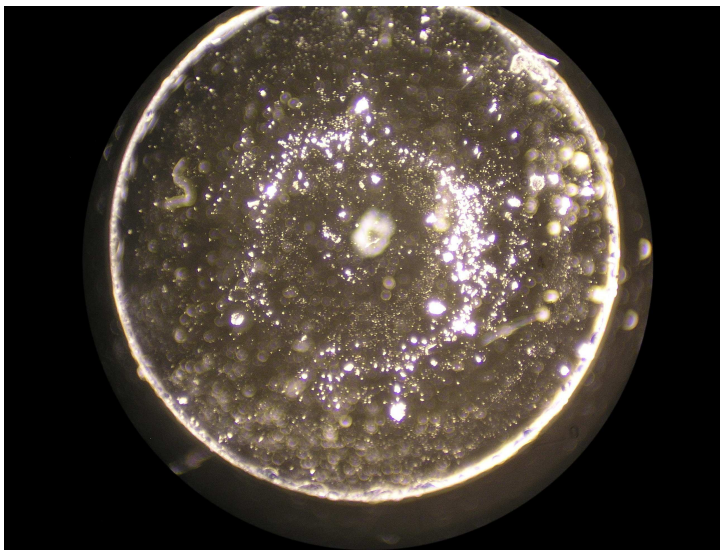

b)

Fig. 3.5.2 Typical condensation of RDX on the surface of quartz glass a) (I) and b), when the laser energy is just below the minimum ignition energy in the case of high confinement. The pressure of argon was 50 bar.

According to the IR-spectroscopic measurements the material of condensation (I) is RDX.[95] It is the same case with the ringlike crystalline rest material (II), which has a radius of 1.5 mm from the centre of quartz glass. The rapid temperature increase of the gas between the RDX pellet and quartz glass causes rapid local increase of pressure. If the temperature increases from 293 K to 473 K (from 20 ^{o}C to 204 ^{o}C), the pressure increases in constant volume from 50 bar to 81 bar.

Figure 3.5.3 depicts a typical laser profile meter image of RDX98/1/1 + 1% C surface in the case of high confinement, when the pressure of argon is 50 bar. The ignition energy of the laser beam is just below the energy of ignition. According to the laser profile meter measurements, the mean volume of the laser evaporated hole in the RDX is typically about 0.1 mm^3. The RDX melted by laser radiation is evaporated and probably the decomposition begins in the vapour phase but is not sufficient to cause an ignition.[96]

The laser evaporated RDX and the gaseous decomposition products rise the local pressure still higher. They will expand because of the pressure difference between the illuminated point of the laser beam and its surrounding and will displace the argon and/or other gases. The level of confinement rises too, as the pressure rises.

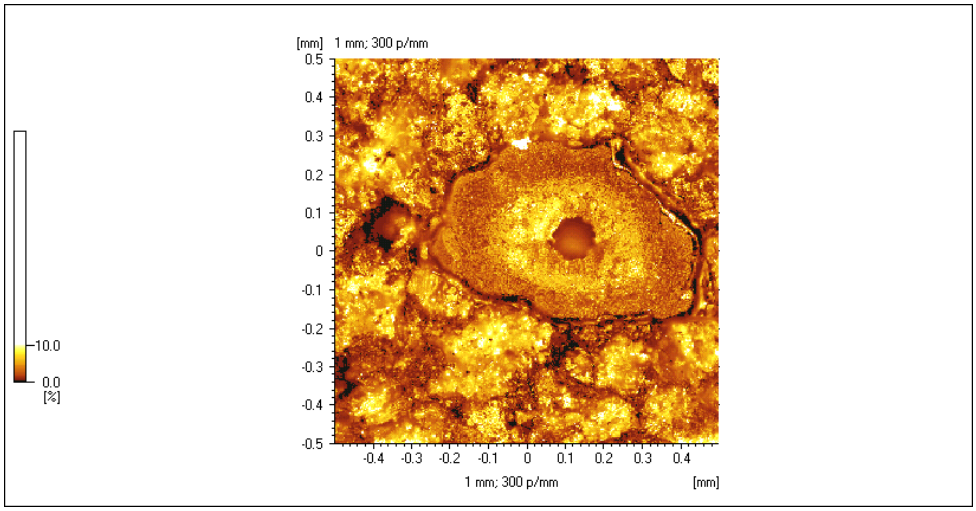

Fig. 3.5.3 A typical surface reflectivity image from a laser profile meter for the RDX98/1/1 + 1% C surface, when the ignition energy of laser beam is just below the energy of ignition in the case of high confinement. The laser evaporated hole is 27 μm in depth and its volume is 0.1 mm^3. The pressure of argon was 50 bar.

Figure 3.5.4 depicts the thermal decomposition rate of solid RDX at temperatures 150 to 190 ^oC and in Figure 3.5.5 the thermal decomposition rate of RDX in a solution of m-nitrobenzene at temperatures 160 to 200 ^oC, respectively. As is typical of many energetic materials, the decomposition accelerates when the temperature rises. According to many references, the decomposition of RDX begins between 160 and 170 ^oC.[96, 97]

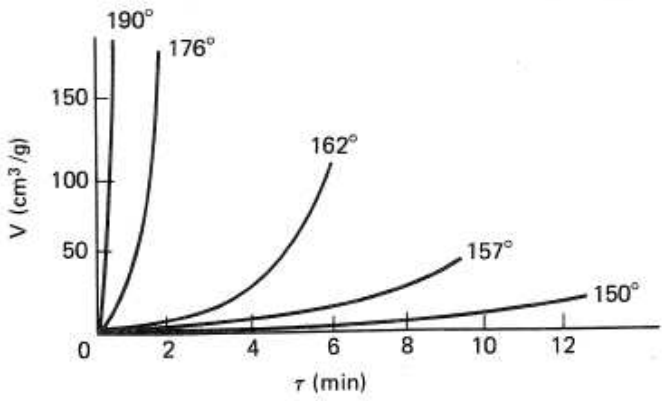

Fig. 3.5.4 Thermal decomposition of solid RDX.[98]

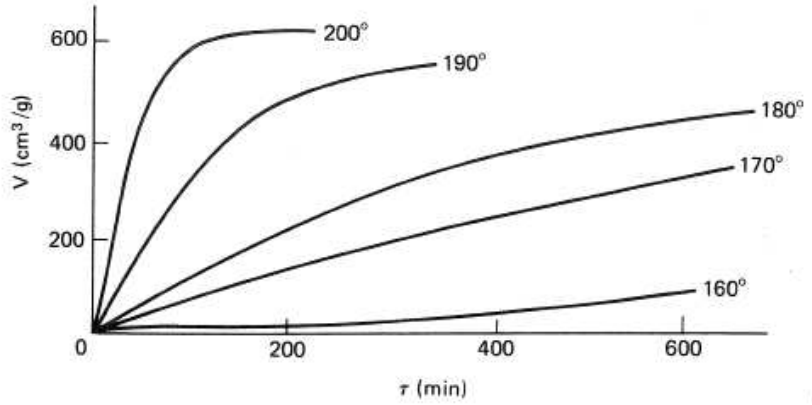

Fig. 3.5.5 Thermal decomposition of RDX in solution of m-nitrobenzene.[98]

Figure 3.5.6 depicts Thermo Gravimetric (TG) and Differential Scanning Calorimetric (DSC) results of RDX as a function of temperature in the range 20 to 340 ^{o}C. According to those results the melting of RDX began in the temperature of 201.6 ^{o}C. All of RDX has melted, by the time 5% of RDX has decomposed.

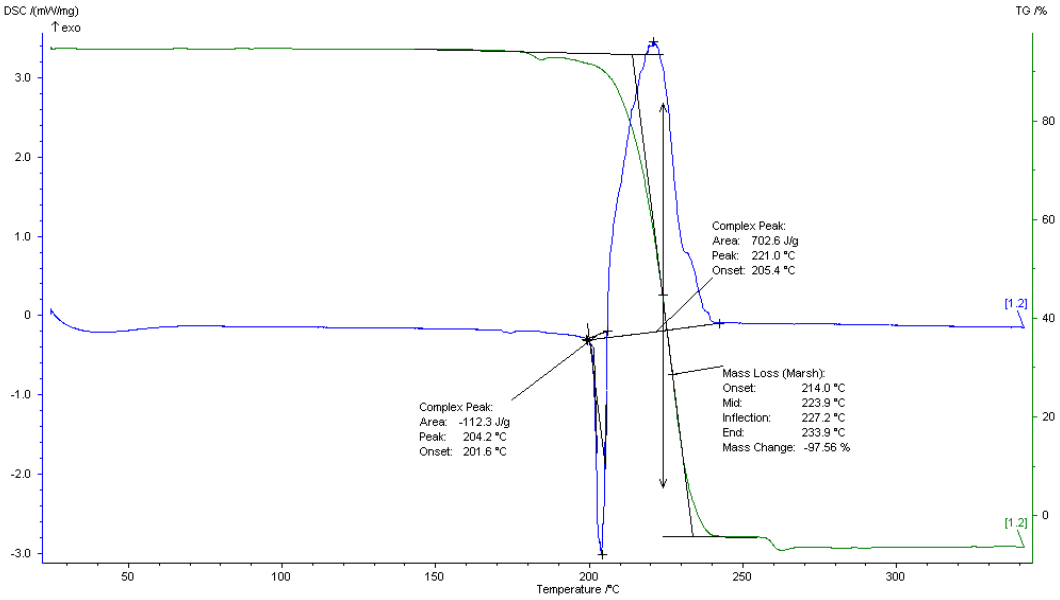

Fig. 3.5.6 Thermo Gravimetric (TG) and Differential Scanning Calorimetric (DSC) results of RDX as a function of temperature in the range 20 to 340 ^{o}C.[99] The temperature rate 5 K/min was used.

Figure 3.5.7 depicts experimental data and its linear fit for the vapour pressure of solid RDX at temperatures from 320 to 375 K (47 to 102 ^{o}C). The function of the fitted line has the form: $P(T) = A + B * T[Pa]$, where $A = -22.6146 \pm 0.29296$ and $B = 0.05558 \pm 8.42613E-4$.[100] The extrapolation for the temperature of 201.6 ^{o}C gives the vapour pressure of RDX as 3.76 Pa and for the temperature of 204 ^{o}C as 3.90 Pa.

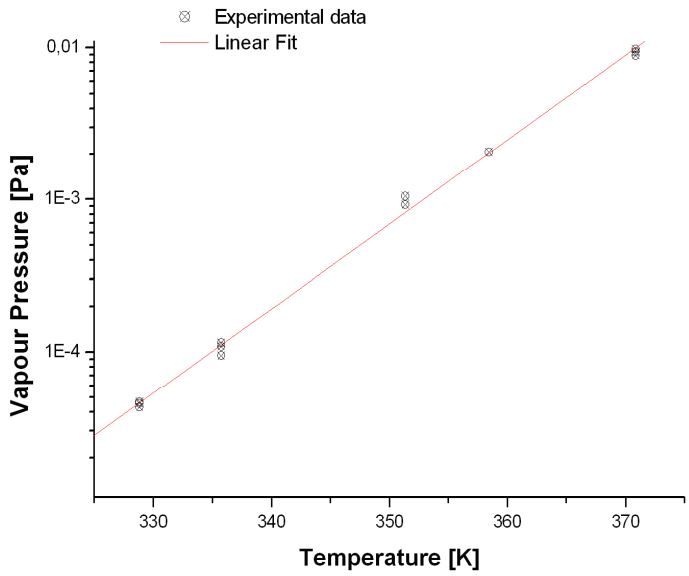

Fig. 3.5.7 Experimental RDX vapour pressure and linear fit.[100]

Authors studying the decomposition of RDX have come to the conclusion that the initial decomposition takes place in the vapour phase and is followed by a more rapid decomposition in the liquid phase.[96, 97, 101] In this mechanism, the result may be deflagration and initiation of detonation by the action of laser radiation. The decomposition of RDX at a fast heating rate is presented in Appendix 2.

Some studies have been carried out on the ignition characteristics of gaseous RDX, by applying the mass and energy conservation equations to a homogeneous mixture in an adiabatic, constant-pressure environment to identify the heat-release mechanisms for achieving ignition and to examine the dependence of ignition delay on the initial temperature and species concentrations.[63, 102] The chemical kinetics scheme involves 49 species and 250 elementary reactions.[103] The formation of CN species gives rise to a luminous flame often serving as an ignition criterion for both experimental and theoretical studies.[63] In all the cases studied in reference[63], ignition occurs only if the initial temperature exceeds 600 K (327 ^{o}C).

The gaseous RDX ignition process can be divided according to some authors into five distinct stages:[63] I Thermal decomposition, II First oxidation, III Chemical preparation, IV Second oxidation, and V Completion stages (Fig 3.5.8), (Appendix 3). In stage I, RDX decomposes to low-molecular weight species such as CH_2O, N_2O, NO_2, HCN and HONO. This decomposition process is slightly endo/exothermic or thermally neutral depending on the initial temperature. In stage II, oxidation reactions occur and release a significant amount of energy, 153 kcal/mol, with the temperature reaching about 1500 K (1227 ^oC). The heat release in stage II is mainly caused by the conversion of CH_2O and NO_2 to H_2O, NO, and CO and, to a lesser extent, by the reactions of HCN and HONO. Stage III represents the chemical preparation time before the second oxidation reactions (Stage IV) take place. The species formed in stage II are relatively stable due to the high activation energies of their associated reactions, and require a finite time to further oxidize. In highly exothermic stage IV, the reduction of HCN and NO to N_2, CO, H_2O, and H_2 is largely responsible for the heat release in Stage IV, at 405 kcal/mol. Finally, all the final products are formed and no further reactions occur in Stage V. If RDX does decompose in the condensed phase during the laser-induced ignition process, the decomposition products at the surface may affect the gas-phase reaction mechanism.[63]

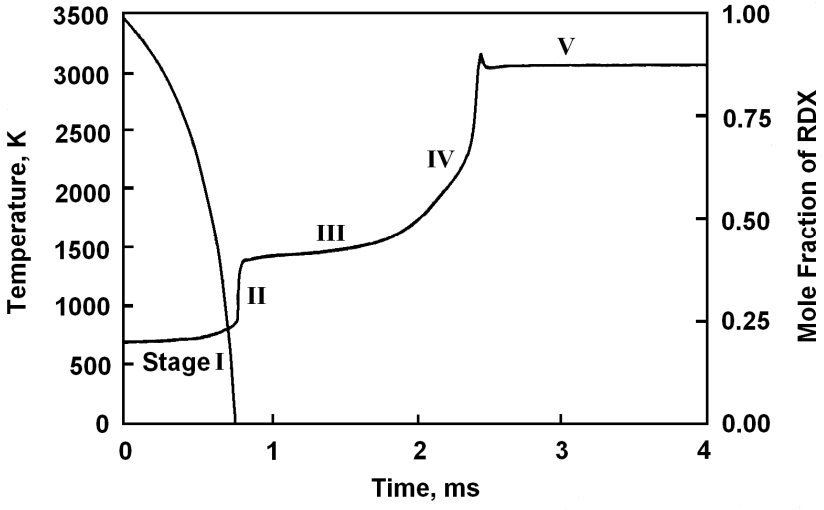

Fig. 3.5.8 Temperature evolution during RDX ignition in well-stirred reactor at P = 1 atm, T_{ini} = 700 K, 100% RDX.[63]

The detailed physiochemical processes involved in the ignition of RDX are schematically illustrated according to Liau et al. in Fig. 3.5.9. The description is in good agreement with the theoretical formulation in the chapter 2.7.

The ignition processes are divided into six distinct stages. The initial temperature of the RDX and the ambient gas is uniformly distributed at room temperature. In the first stage (a) volumetric absorption of laser energy in the solid phase takes place. When the solid reaches its melting temperature, the absorbed radiant energy cannot further raise the temperature without first undergoing a melting process. Since the radiant energy absorbed is insufficient for instantaneous melting of all of the solid within such a short period of time, partial melting of the solid occurs and leads to the formation of a “mushy zone” which consists of both the solid and liquid (b). When a pure liquid layer is formed, the solid-liquid interface starts to move due to the conductive and radiative heat transfer (c). In the liquid, thermal decomposition and subsequent reactions, as well as phase

transition, take place, generating gas bubbles and forming a two phase region. The RDX then undergoes a sequence of rapid evaporation at the surface (d). Ignition occurs if the heat flux is sufficiently large to initiate the subsequent self-accelerated exothermic reactions which result in substantial heat release in the gas phase and emission of light. A luminous flame is produced in the gas phase (e), regressing toward the surface producing hot spots, and finally combusting the RDX (f).[63]

In Fig. 3.5.9 the term t_{id} means the ignition delay time. The term q''_{flux} means the flux of laser light on the surface of RDX. T' means the temperature of ambient gas and T_{ini} means the initial temperature of RDX. T_{melt} is the melting temperature of RDX. The term “Mushy Zone” used means the zone where the solid and the melted RDX form a mixture. The term “Foam Zone” means the zone where the gaseous RDX and the gaseous decomposition products of RDX mix with the melted RDX.

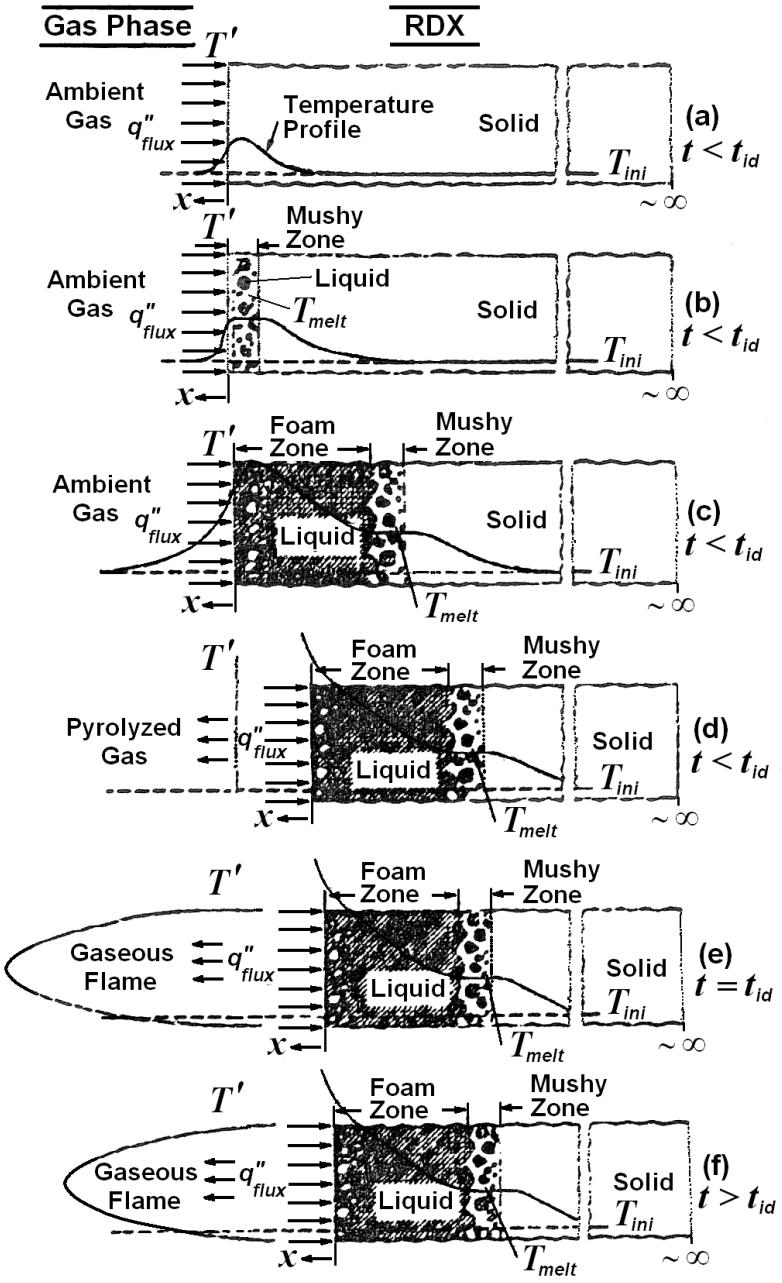

Fig. 3.5.9 Physiochemical processes involved in laser-induced ignition of RDX according Liau et al.[63]

According to the work of Liau et al, the process accelerates to steady-state deflagration in the ambient pressure of 1 atm if the incoming energy is high enough to produce the temperature of 600 K in the zone of pyrolyzed decomposition products and evaporated RDX. According to this work and the works of other authors, Östmark et al., Roman et al. and others, the energy required for ignition is conciderably lower and deflagration accelerates to steady-state detonation, if the ambient pressure is higher and confinement is high enough.

4. Conclusions

A strong dependence between ignition energy and ambient pressure was observed in the diode laser ignition research with RDX and other explosives. For example, in the case of RDX98/1/1+1% carbon black, the measured energy for 95% ignition probability in an ambient pressure of 10 bar was 180 mJ and in an ambient pressure of 50 bar it was 32.6 mJ. Mean ignition energy densities were 29.9 J/cm^2 and 5.4 J/cm^2, respectively. The values have good agreement with the results from other studies on diode lasers and optical fibers[104], but the pressure dependence is stronger in the results of this study, probably because of the higher level of confinement. The pressure dependence at a low pressure is explained by the fact that the reaction rate for a bimolecular reaction in the gas phase is proportional to the pressure squared[79].

Some authors have discovered stronger pressure dependence and lower energy density using the CO_2 laser.[79] An energy density of 1.2 J/cm^2 at 50 bar (5 MPa) was measured using the CO_2 laser in a nitrogen atmosphere and 1.6 J/cm^2 in air.[79] The wavelength used was 10.6 μm (10600 nm), which has higher absorption in the solid RDX when compared with the diode laser wavelength of 808 nm.[63]

Some authors have measured energy density values of 5 to 8 J/cm^2 at 50 bar using the Nd:YAG laser with 532 nm wavelength and 8 ns pulse length[72]. In those experiments, the ignition mechanism was from shock to detonation (SDT). The values are in good agreement with the corresponding energy density values from this study.

The carbon black content dependence of ignition energy is clear between 1% and 3% being 27% lower at 2% carbon black content when compared with the ignition energy of 1% carbon black content, and 31% lower at 3% carbon black content. According to the experiments, the mechanical properties of the RDX

pellet are fragile, using 1% wax content, for 3% or higher carbon black content. Thus the optimum carbon black content may be 1.5 to 2.5%.

According to the diode laser ignition experiments with synthetic air and argon the ignition energies are essentially the same in the same confinement. These results suggest that oxygen (in synthetic air) has no remarkable reactions in the laser illuminated point of the RDX pellet or more generally in the laser illuminated point of any explosive.

For nitrogen, the ignition energies are slightly higher, compared with air (and also with argon) in the same pressure. This is analogous to the CO_2 laser ignition results at lower pressures in the research by Östmark et al., but at higher pressures of air and nitrogen the experimental results of this work are in the reverse order to those of reference[79].

The evaporated RDX and the gaseous decomposition products (for example CH_2O, N_2O, NO_2, HCN and HONO)[63] expand and will displace synthetic air, nitrogen or argon. Initial decomposition takes place in the vapour phase of RDX and on the surface of melted RDX. Highly exothermic reactions begin in the vapour phase and are followed by a more rapid decomposition in the vapour phase and in the liquid phase and the ignition of RDX.[63] The rate of the reactions is deflagration, but it accelerates to the steady state detonation in the environment of high confinement.

According to this study and to those of other authors, the degree of confinement has a strong role in the deflagration to detonation transition ignition mechanism. Using a sufficiently heavy degree of confinement, a closed and tight mechanical structure and sufficiently pressure inside the device, and good absorbance, for example using carbon black in the energetic material, the ignition energy is low enough for economically viable applications of compact diode laser igniters[105, 106] and Appendix 4.

Appendix 1

The Up-and-down method and laser ignition experiments

In true sensitivity experiments it is possible to make only one observation on given specimen. For example, in testing the sensitivity of explosives to shock, a common procedure is to drop a weight on specimens of the same explosive mixture from various heights. There are heights at which some specimens will explode and others will not, and it is assumed that those which do not explode would have exploded were the weight been dropped from a sufficiently great height. It is supposed, therefore, that there is a critical height associated with each specimen and that the specimen will explode when the weight is dropped from a greater height and will not explode when the weight is dropped from a lesser height. The population of specimens is thus characterized by a continuous variable – the critical height, which cannot be measured. All one can do is select some height arbitrarily and determine whether the critical height for a given specimen is less than or greater than the selected height.[94]

For the experiments described above or similar experiments the Up-and-down method and its statistical analysis have been developed, these are described in reference[94]. One important condition is that the variable is normally distributed. The method is effective for estimating the mean. Using the simple statistical analysis, it is possible to estimate the 95 per cent, 50 per cent and 5 per cent points, i.e. the 95 per cent, the mean 50 per cent and the 5 per cent probability of ignition.

Date			02.-03.05.2001							
Wavelength λ[nm]			808							
Pressure P[bar]			30 (synthetic air)							
Explosive			RDX 98/1/1 + 2% C							
Pulse length [ms]			100							
Temperature [ºC]			20							
RH [%]			40							
Num.	**E [mJ] +/-5**	**i**				0	1	2	3	4
		log(h)	3,25	3,27	3,29	3,31	3,33	3,35	3,37	3,39
		h[mA]	1778	1862	1950	2042	2138	2239	2344	2455
1	82									+
2	81								+	
3	80							+		
4	79						+			
5	78					-				
6	79						-			
7	80							-		
8	81								+	
9	80							+		
10	79						-			
11	80							+		
12	79						-			
13	80							-		
14	81								+	
15	80							+		
16	79						-			
17	80							+		
18	79						-			
19	80							+		
20	79						+			
21	78					-				
22	79						+			
23	78					-				
24	79						-			
25	80							+		
26	79						-			
27	80							-		
$\Sigma n_i[+]= 14$		$n_i[+]$				0	3	7	3	1
$\Sigma n_i[-]= 13$		$n_i[-]$				3	7	3	0	0

Table of Appendix 1. Laser ignition experiment for RDX98/1/1 with 2% extra carbon black.

In the laser ignition sensitivity experiments on explosives or on other energetic materials, the diode laser current corresponds to the height in the sensitivity experiments described above. The laser light energy on the surface of a pressed explosive pellet has linear correspondence to the diode laser current (Fig. 3.4.6.). As an example of the use of the up-and-down method for laser ignition research, there are experiments on RDX/1/1 + 2% carbon black in the 30 bar pressure of synthetic air (Table of Appendix 1). The wavelength of the diode laser was 808 nm and the diameter of the optical fibre was 0.8 mm.

Simple statistical analysis[94, 107]

The rule to choose N: $\sum n_i[-]$ = 13 is less than $\sum n_i[+]$ = 14, and so N = 13.

$A = \sum_{i=0}^{k} i n_i = 1 \cdot 7 + 2 \cdot 3 = 13$ and $B = \sum_{i=0}^{k} i^2 n_i = 1 \cdot 7 + 2^2 \cdot 3 = 19$

The mean value has the expression:

$$\overline{X} = y + d\left(\frac{A}{N} \pm 0.5\right) = 3.31 + 0{,}02\left(\frac{13}{13} + 0.5\right) = 3.34,$$

which corresponds to the diode laser current of 2291.5 mA (+0.5 because of N being chosen as the quantity of minus signs). The variable *d* is the expected value of standard deviation (or standard error) and has an advanced estimation with the value of 0.02. The mean value $\overline{X}$ is the 50% confidence interval and so 50% ignition probability too. The standard deviation *s* is written in the form: $s = 1.620d\left(\frac{NB - A^2}{N^2} + 0.029\right) = 1.620 \cdot 0.02(0.462 + 0.029) = 0.0159$. The formula of *s* is an approximation which is quite accurate when $(NB - A^2)/N^2$ is larger than 0.3 but breaks down rapidly when $(NB - A^2)/N^2$ becomes less than 0.3. In this example $(NB - A^2)/N^2 = 0.462 > 0.3$.

The expression of the 5% confidence interval (5% ignition probability) is written in the form: $P_{05} = \overline{X} - z_a \cdot s = 3.34 - 1.645 \cdot 0.0159 = 3.31$, where $z_a = 1.645$ is

chosen from the table of normal deviation. The value 3.31 of P_{05} corresponds to the diode laser current of 2060 mA.

The 95% confidence interval (95% ignition probability) is estimated by $P_{95} = \overline{X} + z_a \cdot s = 3.34 + 1.645 \cdot 0.0159 = 3.366$ corresponding to the diode laser current of 2324 mA.

The example above (Table of Appendix 1) is shortened by the number of tests but describes a typical case of an up-and-down sensitivity experiment well, where the primary advantage is that it automatically concentrates on testing near the mean. According to reference[94] the statistical analysis may be unreliable, when the number of tests is less than 40.

In the laser ignition example, the testing interval of 0.02 is chosen to correspond to the diode laser current of about 100 mA. According to the testing interval analysis[94] the interval should be within the range of about 0.5σ to 2σ, where σ is the standard deviation of the experiment. It is unknown but the value of *s* is a good approximation. So in the case of this example, the interval should be 0.008 to 0.032 and it is 0.02. In the laser ignition experiments described in Chapter 3 the interval used was 0.01, which corresponds to the diode laser current interval of about 50 mA. The number of experiments was usually from 30 to 50, which is in good agreement with the studies of other authors.[79, 107]

Appendix 2

Decomposition of RDX at fast heating rates and its detonation products

The decomposition mechanism of energetic materials, such as nitramines and RDX, are highly dependent upon the chemical environment and the heating rates of the energetic material and may be more complicated than simply unimolecular decomposition.[108, 109] The pathway for unimolecular decomposition of RDX in the case of rapid heating rate is presented in Fig. 1 of Appendix 2. The total energy of chain bond breaking is 262 kcal/mol (4939 kJ/kg). The heat of explosion as computed by the ICT-Thermodynamic code for RDX is 5297 kJ/kg and the heat of detonation is 6322 kJ/kg.[40] The term heat of explosion is used for propellants and heat of detonation for explosives.[14] The decomposition mechanisms of energetic materials and thermochemical modelling applied to decomposition of energetic materials is thoroughly presented in many references.[14, 108, 109]

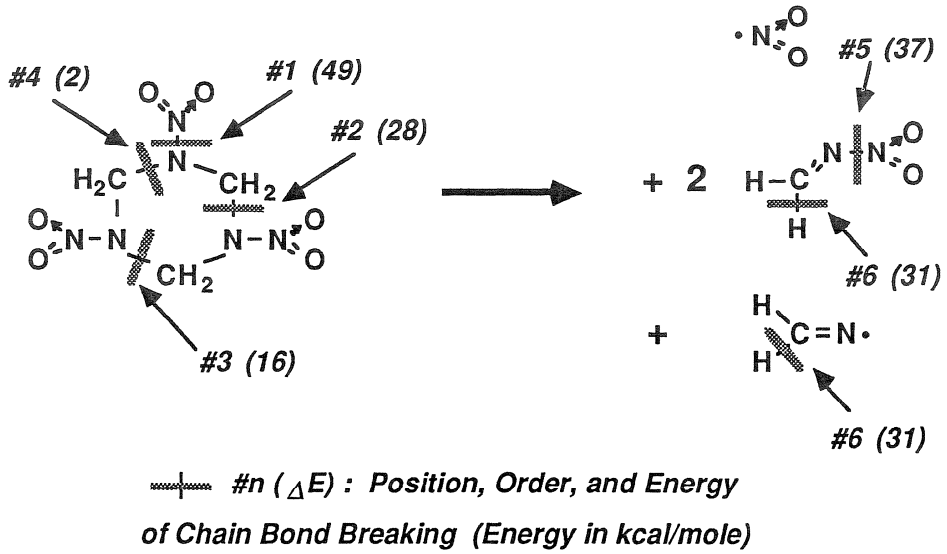

Figure 1 of Appendix 2. Decomposition mechanism for RDX under rapid heating rates. The number indicates the order in which the bonds are broken. The bond breaking energies are given in parentheses in [kcal/mol].[108]

Figure 2 of Appendix 2 depicts the decomposition paths for RDX in the collision-free IR multiphoton decomposition experiment.[110]

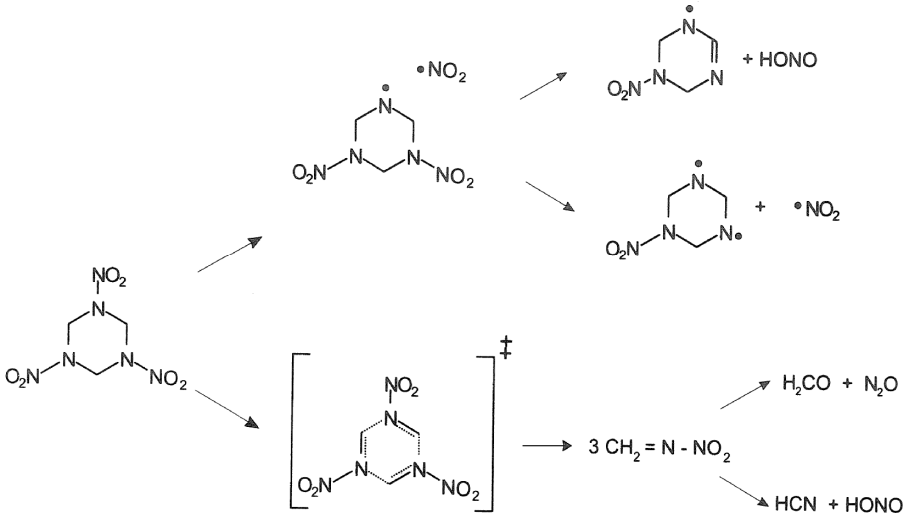

Figure 2 of Appendix 2. Decomposition paths for RDX in the collision-free IR multiphoton decomposition experiment.[110]

The elemental formula of RDX is $C_3H_6N_6O_6$. In the detonation reaction the products of RDX are: $3N_2$, $3H_2O$, and 3CO. In the afterburning reactions CO reacts with oxygen in the air producing CO_2.[14] Heat of combustion of CO is 283.0 kJ/mol (67.59 kcal/mol).[111]

Appendix 3

Decomposition of gaseous RDX in the laser-induced ignition process

In the chemical kinetics studies with gaseous RDX 49 species and 250 elementary reactions have been identified.[112] The formation of CN species as mentioned earlier gives rise to a luminous flame often serving as an ignition criterion for both experimental and theoretical studies.[63] For all the cases studied in reference[63], ignition occurs only if the initial temperature exceeds 600 K (327 ^{o}C).

The gaseous RDX ignition process can be divided into five distinct stages: I Thermal decomposition, II First oxidation, III Chemical preparation, IV Second oxidation, and V Completion stages (Fig 3.6.8). In Stage I, RDX decomposes to low-molecular weight species such as CH_2O, N_2O, NO_2, HCN, and HONO. This decomposition process is slightly endo/exothermic or thermally neutral depending on the initial temperature. In Stage II, oxidation reactions occur and release a significant amount of energy with the temperature reaching about 1500 K (1227 ^{o}C). The dominant net reactions in Stage II can be given as follows:[63]

	$\Delta H[kcal/mol]$
$CH_2O + NO_2 \rightarrow H_2O + NO + CO$	-44
$HNO + HONO \rightarrow H_2O + 2NO$	-23
$2HCN + NO_2 \rightarrow C_2N_2 + NO + H_2O$	-33
$CO + NO_2 \rightarrow CO_2 + NO$	-53
$2HONO \rightarrow NO + NO_2 + H_2O$	+ 8
$2NO_2 \rightarrow 2NO + O_2$	+29

The net heat release is 153 kcal/mol. The heat release in Stage II is mainly caused by the conversion of CH_2O and NO_2 to H_2O, NO, and CO, and to a lesser extent by the reactions of HCN and HONO.[63]

Stage III represents the chemical preparation time before the second oxidation reactions (Stage IV) take place. The species formed in Stage II are relatively stable due to the high activation energies of their associated reactions, and require a finite time to further oxidize. The highly exothermic reactions occurring in Stage IV are according to reference[63] the net reactions:

	$\Delta H[kcal/mol]$
$2HCN + NO \rightarrow 2CO + 2N_2 + H_2$	-158
$N_2O + H_2 \rightarrow N_2 + H_2O$	-78
$C_2N_2 + 2NO \rightarrow CO + 2N_2$	-169

Thus the net heat release is 405 kcal/mol. The reduction of HCN and NO to N_2, CO, H_2O, and H_2 is largely responsible for the heat release in Stage IV. Finally, when all the final products are formed, no further reactions occur in Stage V (Fig 3.6.8).[63] If RDX does decompose in the condensed phase during the laser-induced ignition process, the decomposition products on the surface may affect the gas-phase reaction mechanism.[63]

Laser ignition with mass spectroscopy (LI/MS) has been used to study the pre-ignition/ignition zone of some explosives including RDX.[113] A CO_2 laser has been used to produce the ignition pulse. The main decomposition products have been identified as N_2O, NO, CO_2, N_2, NO_2, HCN, H_2CO and H_2O (for H_2CO the form CH_2O is used in reference[63]). The conclusions mention for example, that HCN and H_2CO play important part in the ignition process of RDX and the ignition of RDX is a multi-phase reaction (involving a gas phase and a condensed phase).

The combination of laser ignition with LIF (Laser Induced Fluorescence) spectroscopy has been used to study the gas phase reactions and decomposition products of RDX.[114] A CO_2 laser has been used to produce the ignition pulse and a Nd:YAG pumped dye laser has been used to monitor the reaction and reaction

products. The technique has been used to measure the relative NO and CN concentrations in the subignition zone of RDX. The calculation of the vibrational temperature in the gas phase reaction zone in the front of sample at subignition has given the temperature of 3100 K, according to authors. The conclusions mention that the Lambert-Beer absorption is the main energy interaction mechanism between a laser beam and a high explosive, but occasionally other unknown absorption process may occur simultaneously.

Appendix 4

Patent of Laser Detonator

References

[1] W. C. Davis, Detonation Physics, Volume1, 1994, Computational Mechanics Associates, Baltimore, MD.

[2] Brish A. A., Galeeva I. A., Zaitsev B. N., Sbitnev E. A. and Tararinstev L. V., Fizika Goreniya i Vzryva, **2**, 3, 132, (1966).

[3] Brish A. A., Galeeva I. A., Zaitsev B. N., Sbitnev E. A. and Tararinstev L. V., Fizika Goreniya i Vzryva, **5**, 4, 475, (1969).

[4] Yang L. C., Menichelli C. F., Sensitivity of Explosives to Laser Energy, California Institute of Technology, Technical Report, 32-1474, (1970).

[5] Yang L. C., Menichelli C. F., Detonation of Insensitive High Explosives by a Q-Switched Ruby Laser, **19**, 473, (1971).

[6] Mikkola E., Wichman I. S., On the Thermal Ignition Of Combustible Materials, Fire and Materials, **14**, 87, (1989)

[7] Mikkola E., Charring of Wood, Technical Research Centre of Finland, Research Reports 689, Espoo, (1990).

[8] Atkins P. W., Physical Chemistry, Fourth Edition, Oxford University Press, (1990).

[9] Laidler K. J., The World of Physical Chemistry, Oxford University Press, (1993).

[10] Meyer R., Koehler J., Homburg A., Explosives, 5th Edition, Wiley-VCH, (2002).

[11] Chapman D. L., Phil. Mag., 47, 90, 1899. M. Jouguet, Sur la propagation des reactions chimiques dans les gaz, Journal de mathematiques pure et appliquees, 60, 347, (1905).

[12] Fickett W., Davis W. C., Detonation Theory and Experiment, Dover Publications, Inc., New York, (2000).

[13] Tokmakoff A., Fayer M. D., Dlott D. D., Chemical Reaction Initiation and Hot-Spot Formation in Shocket Energetic Molecular Materials, J. Phys. Chem., 97, 1901, (1993).

[14] Cooper P. W., Explosives Engineering, Wiley-VCH, Inc., (1996).

[15] Campbell A. W., Davis W. C., Travis J. R., Shock Initiation of Detonation in Liquid Explosives, Physics of Fluids 4, 498, (1961).

[16] Tarver C. M., Combustion and Flame, 46, 157, (1982).

[17] Mader C. L., Numerical Modelling of Detonations, University of California Press, Berkeley, CA, (1979).

[18] Campbell A. W., Davis W. C., Ramsay J. B. and Travis J. R., Shock Initiation of Solid Explosives, Physics of Fluids 4, 511, (1961).

[19] Mader C. L., Forest C. A., Two-Dimensional Homogeneous and Heterogeneous Detonation Wave Propagation, Los Alamos Scientific Laboratory report LA-6259 (1976).

[20] Starkenberg J., An Assessment of the Performance of the Original and Modified Versions of the Forest Fire Explosive Initiation Model, Proceedings Tenth (International) Detonation Symposium, Boston, Massachusetts, July 12 – 16, (1993).

[21] Forest C. A., Burning and Detonation, Proceedings Seventh Symposium (International) on Detonation, Annapolis, Maryland, June 16 – 19, (1981).

[22] Bowman A. L., Forest C. A., Kershner J. D., Mader C. L., Pimbley G. H., Numerical Modeling of Shock Sensitivity Experiments, Proceedings Seventh Symposium (International) on Detonation, Annapolis, Maryland, June 16 – 19, (1981).

[23] Zhao Feng, Sun Chengwei, Chen Peiqi and Ouyang Denghuan, Reaction Rates of PBH-9D Explosive, Proceedings Ninth Symposium (International) on Detonation, Portland, Oregon, August 28 – September 1, (1989).

[24] Liang D., Flis W. J., and Chou P. C., The Calculation of the Constants for the Forest Fire Model, Proceedings Tenth (International) Detonation Symposium, Boston, Massachusetts, July 12 – 16, (1993).

[25] Fedoroff B. T., Sheffield O. E., Encyclopedia of Explosives and Related Items, Picatinny Arsenal Dover, New Jersey, USA, **7,** (1975).

[26] Bowden F. P., Yoffe A. D., Initiation of Growth of Explosions in Liquids and Solids, Cambridge University Press, Cambridge, (1952).

[27] Kelzenberg S., Weiser V., Roth E., Eisenreich N., Berger B. and Haas B., Hot Spot Modeling of Thermite Type Reactions Regarding Particle Size and Composition, 34th International Pyrotechnics Seminar Proceedings, Volume **1**, 81-92, Beaune, France, from october 8 to 11, (2007).

[28] Bowden F. P., Yoffe A. D., Chapters II, III and IV, (1952).

[29] Bowden F. P., Yoffe A. D., Chapters IV, V and VII, (1958).

[30] Bowden F. P., Proceedings of 9th International Symposium on Combustion, p 499-515, Academic Press, (1963).

[31] Mader C. L., Phys Fluids 6 (3) 375 (1963) and CA 58, 8844, (1963).

[32] Mader C. L., Phys Fluids 8 (10) 1811 (1965) and CA 63, 16120, (1965).

[33] Mader C. L., Proceedings of 5th Symposium on Detonation, p 177, (1970).

[34] Blackburn J.H. and Seely L. B., Trans Farad Soc 61, 537, (1965) and CA 62, 8924, (1965).

[35] Kholevo, Proceedings International Conference on Sensitivity and Hazards of Explosives, p 5 – 26, London, (1963).

[36] Andreev, Proceedings International Conference on Sensitivity and Hazards of Explosives, p 47 – 151, London, (1963).

[37] Afanas'ev, Bobosev, Initiation of Solid Explosives by Impact, Acad. Sc. USSR, (1968), (Translation 19).

[38] Urbanski T., Chemistry and Technology of Explosives, Vol 1, Pergamon Press, Oxford, (1983).

[39] Finnish Defence Forces Technical Research Centre, Results in the Research of Explosive Technology Laboratory.

[40] Mayer R., Köhler J., Homburg A., Explosives, Wiley-VCH Verlag GmbH, Weinheim, (2002).

[41] Afanas'ev, Bobolev, Initiation of Solid Explosives by Impact, Acad. Sc. USSR, (1968).

[42] Johnson J. N., Tang P. K., Forest C. A., Shock-wave initiation of heterogeneous reactive solids, J. Appl. Phys., **57**, 9, 4232, (1985).

[43] Lee E. L., Tarver C. M., Phenomenological Model of Shock Initiation in Heterogeneous Explosives, Phys. Fluids, **23**, 12, 2362, (1980).

[44] Lee E. L., Hornig H. C., Kury J. W., Lawrence Livermore Laboratory Report UCRL-50422, (1968).

[45] Taylor B. C., Ervin L. H., Separation of ignition and buildup to detonation in pressed TNT, Proceedings Sixth Symposium (International) on Detonation, ARC-221, Office of Naval Research-Department of the NAVY, p. 3, Coronado, California, (1976).

[46] Tarver C.M., Breithaupt R. D., Kury J. W., Current Experimental and Theoretical Understanding of Detonation Waves in Heterogeneous Solid Explosives, International Synposium on Pyrotechnics and Explosives, 692, Beijing, China, 12 – 15 October (1987).

[47] Tarver C. M., Ignition and Growth Modelling of LX-17 Hockey Puck Experiments, Propellants, Explosives, Pyrotechnics, **30**, 2, 109, (2005).

[48] Tarver C. M., Hallquist J. O., Erickson L. M., Modeling Short Pulse Duration Shock Initiation of Solid Explosives, Proceedings 8th Symposium (International) on Detonation, Naval Surface Weapons Center NSWC MP 86-194, p. 951, Albuquerque, NM, 15 – 19 July (1985).

[49] Green L. G., Tarver C. M., Erskine D. J., Reaction Zone Structure in Supracompressed Detonating Explosives, Proceedings 9th Symposium

(International) on Detonation, Office of the Chief of Naval Research OCNR 113291-7, p. 670, Portland, OR, August 28 – September 1 (1989).

[50] Tarver C. M., Kury J. W., Breithaupt R. D., Detonation Waves in Triaminotrinitrobentzene, J. Appl. Phys., **82**, 3771, (1997).

[51] Tarver C. M., Parker N. L., Palmer H. G., Hayes B., Erickson L. M., Reactive Flow Modeling of Recent Embedded Gauge and Metal Acceleration Experiments on Detonating PBX 9404 and LX-17, J. Energ. Mater., **1**, 213, (1983).

[52] Sheffield S. A., Bloomquist D. D., Tarver C. M., Subnanosecond Measurements of Detonation Fronts in Solid High Explosives, J. Chem. Phys., **80**, 3831, (1984).

[53] Tarver C. M., Maiden D. E., Experimental Measurements and Numerical Simulations of Metal Spallation by Detonating Solid Explosives, Shock Waves in Condensed Matter-1987, Elsevier Science Publishers B. V., New York, p. 363, (1988).

[54] Tarver C. M., Modeling Shock Initiation and Detonation Divergence Tests on TATB-Based Explosives, Propellants, Explosives, Pyrotechnics, **15**, 132, (1990).

[55] Tarver C. M., Tao W. C., Lee C. G., Sideways Plate Push Test for Detonating Solid Explosives, Propellants, Explosives, Pyrotechnics, **21**, 238, (1996).

[56] Tarver C. M., Breithaupt R. D., Kury J. W., Detonation Waves in Pentaerythritol Tetranitrate, J. Appl. Phys., **81**, 7193, (1997).

[57] Kury J. W., Breithaupt R. D., Tarver C. M., Detonation Waves in Trinitrotoluene, Shock Waves, **9**, 227, (1999).

[58] Kovalskii A. A., Khlevnoi S. S., Mikheev V. F., Fizika Goreniya I Vzryva, **3**, 527, (1967).

[59] Srakovskii L. G., Frolov E. I., Fizika Goreniya I Vzryva, **16**, 140, (1980).

[60] Frank-Kamenetskii D. A., Calculation of Thermal Explosion Limits, Acta Physicochimica U.R.S.S., 10, 365, (1939).

[61] von Allmen M., Blatter A., Laser Beam Interactions with Materials: Physical Principals and Applications, Springer, New York, (1995).

[62] Silfvast W. T., Laser Fundamentals, 316, Cambridge University Press, (1999).

[63] Liau Y. -C., Kim E. S. and Yang V., A comprehensive analysis of laser-induced ignition of RDX monopropellant, CPIA Pupl. 2000, 701 (JANNAF 37th combustion subcommittee meeting, 2000, Vol 1).

[64] Krause G., Stationary Theory of Heat Explosion, Proceedings 38th International Annual Conference of ICT, June 26 – 29, Karlsruhe, Federal Republic of Germany, 18-1 – 18-12, (2007).

[65] Krause G., Theory of Heat Explosion, 2. Symposium in Theory of Heat Explosion, Chem. Kinetics and Calorimetry, Potsdam, (2007).

[66] Bellamy, Anthony, A method for production of HNS II, European Patent, EPO0277386, Assignee: Bofors Explosives AB (Karlsskoga, S-691 86, SE), Application number: EP19870202613, 14.06.1995.

[67] Dobratz B. M., LLNL Handbook of Explosives, UCRL-52997, Lawrence Livermore National Laboratory, (1981).

[68] Brish A. A., Galeeva I. A., Zaitsev B. N., Sbitnev E. A. and Tararinstev L. V., Fizika Goreniya i Vzryva, **2**, 3, 132, (1966).

[69] Brish A. A., Galeeva I. A., Zaitsev B. N., Sbitnev E. A. and Tararinstev L. V., Fizika Goreniya i Vzryva, **5**, 4, 475, (1969).

[70] Yang L. C., Menichelli C. F., Sensitivity of Explosives to Laser Energy, California Institute of Technology, Technical Report, 32-1474, (1970).

[71] Yang L. C., Menichelli C. F., Detonation of Insensitive High Explosives by a Q-Switched Ruby Laser, **19**, 473, (1971).

[72] Botcher T. R., Ladouceur H. D. and Russell T. P., Pressure Dependent Laser Induced Decomposition of RDX, Shock Compression of Condenced Matter - 1997, The American Institute of Physics, 989-992, (1998)

[73] Renlund A. M., Stanton P. L. and Trott W. M., Laser initiation of secondary explosives, Proceedings Ninth Symposium (International) on Detonation, Portland, Oregon, August 27 – September 1, 1118-1127, (1989).

[74] Marchand A. and Bigot C., Solid-state Laser Initiation System for Defense Application, 34th International Pyrotechnics Seminar Proceedings, Volume **2**, 679-689, Beaune, France, from october 8 to 11, (2007).

[75] Moulard H., Ritter A. and Mory J., Studies on Working Time Reproducibility of a Laser Ignited Detonator, 34th International Pyrotechnics Seminar Proceedings, Volume **2**, 667-677, Beaune, France, from october 8 to 11, (2007).

[76] Sofue T., Iwama A., Ignition of Composite Propellant at Subatmospheric Pressures by means of Carbon Dioxide Laser, Propellants and Explosives, **4**, 98-106, (1979).

[77] Harayama M., Saito T., Iwama A., Ignition of Composite Propellant at Subatmospheric Pressures, Combustion and Flames, **52**, 81-89 (1983).

[78] Östmark H., Laser as Tool in Sensitivity Testing of Explosives, Proceedings 8th Symposium on Detonation, 473-484, NSWC 86-194, Albuquerque, New Mexico, July 15-19, (1985).

[79] Östmark H. and Gräns R., Laser Ignition of Explosives: Effects of Gas Pressure on the Threshold Ignition Energy, Journal of Energetic Materials, **8**, 4, 308-322, (1990).

[80] Östmark H., Roman N., Laser Ignition of Explosives: Pyrotechnic Ignition Mechanisms, Journal of Applied Physics, **73**, 4, 1993-2003, (1993).

[81] Kuo K. K., Kim J. U., Fetherolf B. L., Torikai T., Preignition Dynamics of RDX-Based Energetic Materials Under CO_2 Laser Heating, Combustion and Flame, **95**, 351 – 361, (1993).

[82] Östmark H., Carlson M. and Ekvall K., Laser Ignition of Explosives: Effects of Laser Wavelength on the Threshold Ignition Energy, Journal of Energetic Materials, **12**, 63-83, (1994).

[83] Kunz S. C., Salas F. J., Diode Laser Ignition of High Explosives and Pyrotechnics, Sandia National Laboratories, SAND—87-3032C, DE88 008771, (1988).

[84] Ewick D. W., Beckman T. M., Holy J. A. and Thorpe R., Ignition of HMX Using Low Energy Laser Diodes, EG&G Mound Applied Technologies, MLM--3628-OP DE90 007637 (1990).

[85] Glass M. W., Merson J. A., Salas F. J., Modeling low Energy Laser Ignition of Explosive and Pyrotechnic Powders, Sandia National Laboratories, SAND—92-0249C, DE88 015000, (1992)

[86] Petterson A., Petterson J. and Roman N., Diode Laser Ignition of Unconfined Secondary Explosive: A Parametric Study, Proceedings 11th (International) Detonation Symposium, Snowmass, Colorado, August 30 – September 4, (1998).

[87] Dilhan D., Moulard H., Ritter A. and Castarede M., Overview of Recent Developments of Laser Initiated Detonator for Space Applications, 34th International Pyrotechnics Seminar Proceedings, Volume **2**, 657-666, Beaune, France, from october 8 to 11, (2007)

[88] Harrach R. J., Journal of Applied Physics, **47**, 2473, (1976)

[89] Chernai A. V., Fizika Goreniya I Vzryva, **18**, 48, (1982)

[90] Atwood A. I., Price C. F., Boggs T. L. and Richter H. P., Transient Combustion Analysis of Energetic Materials, Proceedings 19th International Annual Conference of ICT, June 29 – July 1, Karlsruhe, Federal Republic of Germany, I-1, (1988).

[91] Price C. F., Atwood A. I. and Boggs T. L., An Improved Model of the Deflagration-to Detonation Transition in Porous Beds, Proceedings Ninth Symposium (International) on Detonation, August 28 – September 1, Portland, Oregon, **I**, 363 – 376, (1989).

[92] Gillard Ph, and Roux M., Ignition of Pyrotechnic Mixture by means of Laser Diode, Part I: Numerical Modeling, Propellants, Explosives, Pyrotechnics, **22**, 256-262, (1997)

[93] Rubenchik A., M., On the Initiation of High Explosives by Laser Radiation, Propellants, Explosives, Pyrotechnics, **32**, 4, 296-300, (2007)

[94] Dixon W. J., Massey, Jr. F. J., Introduction to Statistical Analysis, Second Edition, McGraw-Hill Book Company, Inc., New York, (1957)

[95] Toivanen T.-J., Analyse report 08/129/D/I of Defence Forces Technical Research Centre, 14.2.2008.

[96] Urbanski T., Chemistry and Technology of Explosives, Vol 4, 374, Pergamon Press, Oxford, (1983)

[97] Debenham D. F. and Owen A. J., Proceedings of Fourth Symposium on Stability of Explosives, 201, Mölle, 1976.

[98] Maksimov Yu. Ya., in, Theory of Explosives (Ed. Andreev K. K.), 73, Collective vol., Vysshaya Shkola, Moscow, 1967.

[99] Hihkiö M., Vormisto T., TG and DSC measurements of pure RDX, Finnish Defence Forces Technical Research Centre, PVTT, Explosives Technology, 2003.

[100] Rosen J. M., Dickinson C., Vapour Pressures and Heats of Sublimation of Some High Melting Organic Explosives, J. Chem. Eng. Data **14**, 120 - 124, 1969

[101] Cosgrave J. D. and Owen A. J., Comb. & Flame **22**, 13, 19 (1974)

[102] Strakouskiy L., Cohen A., Fifer R., Beyer R. and Forch B., Laser Ignition of Propellants and Explosive, ARL-TR-1699, Army Research Laboratory, Aberdeen Proving Ground, MD, (1998).

[103] Kim E. S., Ph.D. Thesis, The Pennsylvania State University, Department of Mechanical and Nuclear Engineering, (2000).

[104] Roman N., Pettersson A., Pettersson J. and Bergman H., Diode laser ignition of RDX 98/1/1, Proceedings 33th International Annual Conference of ICT, June 25 – 28, Karlsruhe, Federal Republic of Germany, 26-1 – 26-16, (2002).

[105] Harkoma M., Hihkiö M. and Vormisto T., Laser Detonator, European Patent Office, EP 1 443 297 B1, DE, FR, GB, SE, Proprietor PVTT, Application number: 04397005.2, Bulletin 2008/43, 22.10.2008.

[106] Harkoma M., Hihkiö M. and Vormisto T., DDT-tyypin lasersytytin, Laserdetonator av DDT-typ, Patentti ja rekisterihallitus, FI 112702 B, Haltija PVTT, F42C 19/00, 31.12.2003.

[107] Discussions with Roman N., Pettersson J. and Pettersson A. in FOI Department of Energetic Materials, Grindsjön in Autumn1997.

[108] Melius C. F., Thermocemical Modeling: I. Application to Decomposition of Energetic Materials. An article in the book: Bulusu S. N., Chemistry and Physics of Energetic Materials, Kluwer Academic Publishers, 1990, and references therein.

[109] Östmark H., Bergman H., Ekvall K., Langlet A., A study of the sensitivity and decomposition of 1,3,5-trinitro-2-oxo-1,3,5-triazacyclo-hexane, Thermochimica Acta, **260**, 201-216, (1995).

[110] Zhao X., Hintsa E. J., Lee Y. T., J. Chem Phys., **88**, 801, (1988).

[111] Lide D. R., CRC Handbook of Chemistry and Physics, 73rd Edition, CRC Press, Boca Raton, Florida (1992 - 1993).

[112] Kim E. S., Ph.D. Thesis, The Pennsylvania State University, Department of Mechanical and Nuclear Engineering, (2000).

[113] Östmark H., Bergman H., Ekvall K., Laser pyrolysis of explosives combined with mass spectral studies of the ignition zone, Journal of Analytical and Applied Pyrolysis, **24**, 163, (1992).

[114] Östmark H., Carlson M., Ekvall K., Concentration and Temperature Measurements in the Laser-Induced High Explosive Ignition Zone. Part I: LIF Spectroscopy Measurements, Combustion and Flames, **105**, 381, (1996).